FeRIC-based magnetogenetics: evaluation of methods and protocols in *in vitro* models

Miriam Hernández-Morales[1,2], Victor Han[1,2], Richard H Kramer[3], Chunlei Liu[1,2]*

[1]Department of Electrical Engineering and Computer Sciences, University of California, Berkeley, CA 94720, USA
[2]Helen Wills Neuroscience Institute, University of California, Berkeley, CA 94720, USA
[3]Department of Molecular and Cell Biology, University of California, Berkeley, Berkeley, CA 94720, USA

Figures: 3; Supplemental Figures: 5

Corresponding address:

*Chunlei Liu, PhD
505 Cory Hall MC# 1770
University of California, Berkeley, CA 94720, USA
Email: chunlei.liu@berkeley.edu
Tel: (510)664 7596

Abstract

FeRIC (Ferritin iron Redistribution to Ion Channels) is a magnetogenetic technique that uses radiofrequency (RF) waves to activate the transient receptor potential channels, such as TRPV1 and TRPV4, coupled to cellular ferritins. In cells expressing ferritin-tagged TRPV, RF stimulation increases the cytosolic Ca^{2+} levels via a biochemical pathway. The interaction between RF and ferritin increases the free cytosolic iron level that in turn, triggers chemical reactions producing reactive oxygen species and oxidized lipids that activate the ferritin-tagged TRPV. In this pathway, it is expected that experimental factors that disturb the ferritin expression, the ferritin iron load, the TRPV functional expression, or the cellular redox state will impact the RF efficacy to activate ferritin-tagged TRPV. Here, three *in vitro* protocols were compared for using FeRIC to remotely activate ferritin-tagged TRPV. Further, several experimental factors were examined that either enhance or abolish the RF control of ferritin-tagged TRPV. The findings may help establish reproducible magnetogenetic experimental protocols.

Introduction

Magnetogenetic techniques have been developed as promising tools to noninvasively and remotely control cell activity. For example, static, low frequency or radiofrequency (RF) magnetic fields can activate transient receptor potential vanilloid channels (TRPV) coupled to ferritin (Duret et al., 2019; Hernández-Morales et al., 2020; Hutson et al., 2017; Stanley et al., 2016; Wheeler et al., 2016). The biophysical mechanisms responsible for magnetic activation of the channels is still being worked out. It was first proposed that the interaction between magnetic fields and ferritins produces heat or mechanical stimuli that directly activate TRPV1 and TRPV4, which are intrinsically temperature- and mechanically-sensitive (Stanley et al., 2016; Wheeler et al., 2016). However, no change in temperature could be detected upon RF exposure either at the surface of ferritin or in surrounding fluid (Davis et al., 2020). Additionally, theoretical calculations of the temperature change produced by RF are inconsistent with this model (Barbic, 2019; Duret et al., 2019; Meister, 2016). Recently, we proposed an indirect biochemical mechanism that allows RF waves to activate ferritin-tagged TRPV. Specifically, by triggering dissociation of iron from the ferritin, RF catalyzes the generation of reactive oxygen species (ROS) and oxidized lipids, which are activators of TRPV (Hernández-Morales et al., 2020). This biochemical pathway and the role of ROS in the RF-induced activation of ferritin-tagged TRPV has been recently corroborated (Brier et al., 2020)

Besides the uncertainties about the underlying mechanisms, the efficacy of a specific magnetogenetic technique that uses a ferritin-fused TRPV4, named Magneto, has also been questioned (Kole et al., 2019; Wang et al., 2019; Xu et al., 2019). In both theoretical and experimental studies, multiple factors could produce discrepancies, including the variability of the components of the magnetogenetic techniques. For example, in theoretical calculations, whereas one study assumed ferritin contains ~2400 iron atoms and it is paramagnetic (Meister, 2016), another study assumed ferritin contains ~4500 iron atoms and it is superparamagnetic (Barbic, 2019). In experimental studies, different magnetogenetic approaches use diverse magnetic fields (static, low frequency, or RF at kHz or MHz ranges) and have tagged TRPV with both endogenous or chimeric ferritin (Duret et al., 2019; Hernández-Morales et al., 2020; Hutson et al., 2017; Stanley et al., 2016; Wheeler et al., 2016). The level of ferritin iron load and the functional expression of both ferritin and TRPV also may influence the efficacy of the magnetogenetics techniques. Ideally, ferritins should be at the maximum iron load to transduce magnetic fields proficiently. However, it is unknown if the chimeric ferritins store iron at the same

level as endogenous ferritins. Furthermore, the iron load of endogenous ferritin is highly variable, from empty to maximum load (~4500 iron atoms) (Jian et al., 2016). Regarding TRPV, those channels should be functionally expressed at the cell membrane. However, their expression and sensitivity to diverse stimuli are subjected to cellular regulatory mechanisms. Several TRPV channels are constitutively active and cells prevent the associated cytotoxic effect by downregulating the TRPV density at the plasma membrane (Montell, 2004; Planells-Cases and Ferrer-Montiel, 2007).

Given the many potential variables described above, we reasoned that experimental factors that disturb the cellular iron homeostasis and the ferritin and TRPV channels expression, may impact the magnetic control of ferritin-tagged TRPV. Using the FeRIC approach we examined the influence of diverse experimental factors on the efficacy of RF to induce Ca^{2+} responses in cells expressing $TRPV4^{FeRIC}$. We found that some factors may abolish the magnetic control of ferritin-tagged TRPV, but the response can be rescued with some other procedures. The observations reported here may contribute to the standardization of the current magnetogenetic in vitro experimental techniques.

Results

Experimental factors affect the RF efficacy to induce Ca^{2+} responses in cells expressing $TRPV4^{FeRIC}$

The effects of different experimental factors on the RF-induced activation of ferritin-tagged TRPV4 were examined using the FeRIC system. RF waves at 180 MHz and 12 μT were generated with solenoid coils covering a cell culture dish (**Fig. S1**). The cytosolic Ca^{2+} levels were monitored in Neuro2a (N2a) cells expressing GCaMP6 (GCaMP6) plus $TRPV4^{FeRIC}$. The cells expressing $TRPV4^{FeRIC}$ were identified as mCherry positive cells, which is the reporter included in the $TRPV4^{FeRIC}$ construct. Data were quantified as the change in GCaMP6 fluorescence divided by baseline fluorescence ($\Delta F/F0$) and the area under the curve (AUC). GCaMP6 data are presented as the AUC averages (± SEM) from all $TRPV4^{FeRIC}$-expressing cells. A cell was considered responsive to RF when the GCaMP6 $\Delta F/F0$ increased 10 times over the standard deviation of its baseline fluorescence (see Materials and methods).

I. RF-induced Ca^{2+} responses in $TRPV4^{FeRIC}$-expressing N2a cells decreases with longer periods of $TRPV4^{FeRIC}$ transient expression.

To evaluate the influence of the time delays between seeding, transfection, and functional expression of $TRPV4^{FeRIC}$, we examined three different timing protocols (**Fig. 1A**) that correspond to those reported for magnetic control of ferritin-tagged TRPV (Hernández-Morales et al., 2020; Hutson et al., 2017; Stanley et al., 2016; Wheeler et al., 2016). As previously reported, RF stimulation does not change the cytosolic Ca^{2+} levels in N2a cells expressing only GCaMP6. In contrast, in N2a cells imaged 24-h after transfection with $TRPV4^{FeRIC}$ plus GCaMP6 (timing protocol 1, 24-h post-transfection), RF stimulation (180 MHz, 12 μT) increased the GCaMP6 AUC with respect to unstimulated cells (**Fig. 1B, S2A, table S1**; No RF: -17.4 ± 6.2; RF: 226.4 ± 31.4; $p<0.0001$). In contrast, in $TRPV4^{FeRIC}$-expressing N2a cells imaged 48 or 72-h post-transfection (timing protocols 2 and 3, respectively), RF stimulation did not increase the GCaMP6 fluorescence relative to unstimulated cells (**Fig. 1B, S2A, table S1**; No RF 48-h: 8.5 ± 12.8; RF 48-h: 95.5 ± 34.1; No RF 72-h: 21.1 ± 5.8; RF 72-h: 48.2 ± 26.2). For all experiments, the functional expression of $TRPV4^{FeRIC}$ was corroborated with the TRPV4 agonist GSK 1016790A (GSK101) at 1 μM, which is a saturating concentration that ensures the maximum

activation of TRPV4^{FeRIC} (**Fig. S2A**). Moreover, the RF-induced activation of TRPV4^{FeRIC} was inhibited with the TRPV4 antagonist GSK 2193874 (GSK219, 1 μM; **Fig. 1B, S2A**).

To corroborate the expression of FeRIC channels at the cell membrane, we examined the permeability of N2a cells expressing TRPV4^{FeRIC} to Yo Pro 1, which is a large cation that binds to DNA. TRPV are cation channels permeable to Na^+, K^+, and Ca^{2+}; however, after continuous agonist stimulation, some members of the TRPV family become permeable to larger cations, such as Yo Pro 1, due to a pore dilation process (Banke et al., 2010; Ferreira and Faria, 2016; McCoy et al., 2017). Stimulation with GSK101 at 50 nM for 20 min of TRPV4^{FeRIC}- and TRPV4^{WT}-expressing N2a cells (at 24 h post-transfection) produced Yo Pro 1 influx in about 20 - 30% of examined cells (**Fig.1 D, E, S3**; TRPV4^{FeRIC}: 21.3 ± 2.9 %, n = 3723 cell, 4 independent experiments; TRPV4^{WT}: 32.4 ± 3.7 %, n = 3470 cells, 5 independent experiments). In contrast, Yo Pro 1 influx was not observed in mock-transfected N2a cells (1.3 ± 0.2 %, n =3001 cells, 4 independent experiments) or in TRPV4^{FeRIC}- expressing N2a cells in the absence of GSK101 (no stimulus: 0.3 ± 0.1 %, n = 3448 cells, 4 independent experiments) or in the presence of the TRPV4 antagonist GSK219 (3.1 ± 2.2 %, n =1388 cells, 3 independent experiments) (**Fig.1 D, E, S3**).

Those results indicate that in N2a cells, the transgene expression of TRPV4^{FeRIC} results in its functional expression at the cell membrane. However, longer periods of TRPV4^{FeRIC} expression in N2a cells decrease their responsiveness to RF. That effect could be due to 1) a progressive decrease in the efficacy of ferritin as a RF transducer, 2) the functional downregulation of TRPV4^{FeRIC}, 3) disturbance in the coupling between ferritin and TRPV4^{FeRIC}, or 4) the combination of all those effects. Although it is unclear the cause of the loss of RF responsiveness over time, it is essential to determine the optimal time for expression of these channels when implementing magnetogenetic techniques with transient transfection.

II. Increasing the cellular iron import enhances the RF efficacy to induce Ca^{2+} responses in cells expressing TRPV4^{FeRIC}.

The potency of ferritin as the RF transducer depends on its iron load. To test if ferritin iron load is involved in the TRPV4^{FeRIC} responsiveness to RF, TRPV4^{FeRIC}-expressing N2a cells were treated with holotransferrin (0.5 mg/mL) to increase the cellular iron import. Holotransferrin is an iron transport protein that delivers iron into cells after binding to its receptor on the cell membrane (Giometto et al., 1993). RF stimulation significantly increased the GCaMP6 AUC in TRPV4^{FeRIC}-expressing N2a cells treated with holotransferrin imaged at 24, 48 and 72-h post-transfection relative to unstimulated cells (**Fig. 1C, S2B, table S1**; No RF 24-h: 31 ± 9.5; RF 24-h: 520 ± 50.2; No RF 48-h: -0.5 ± 7.3; RF 48-h: 260.6 ± 52.3; No RF 72-h: -1.2 ± 4.8; RF 72-h: 550.1 ± 50; $p<0.0001$). Notably, in TRPV4^{FeRIC}-expressing N2a cells imaged 72-h after transfection, holotransferrin treatment produced about a 10-fold increase in the RF-induced increase of GCaMP6 AUC relative to non-treated cells.

Those results indicate that increasing cellular iron import enhances the RF-induced Ca^{2+} responses in cells expressing TRPV4^{FeRIC}. On the other hand, it is possible that the loss of RF responsiveness in TRPV4^{FeRIC}-expressing N2a cells over time might be associated with a progressive ferritin iron depletion. Nevertheless, previously we showed that expression of FeRIC channels for periods up to 72-h did not alter the cellular iron bioavailability (Hutson et al., 2017), suggesting that any potential progressive iron depletion, if it occurs, is limited to those ferritins coupled to FeRIC channels. This observation can be used to improve the magnetic control of

ferritin-tagged TRPV in *in vitro* models because it is feasible to experimentally increase the cellular iron import.

III. Abolishing the temperature sensitivity of TRPV4^{FeRIC} and lowering the extracellular Ca^{2+} levels prevent the functional downregulation of ferritin-tagged TRPV.

Because some TRPV channels are constitutively active, cells prevent the cytotoxic effect of excessive Ca^{2+} influx by regulating their expression at the cell membrane (Bezzerides et al., 2004; Ferrandiz-Huertas et al., 2014; Montell, 2004; Planells-Cases and Ferrer-Montiel, 2007; Sanz-Salvador et al., 2012a; Shukla et al., 2010). Diverse factors modulate the TRPV4 recycling from the cell membrane to cytosolic vesicles including temperature, continuous stimulation with agonists, extracellular Ca^{2+} levels, among others (Baratchi et al., 2019; Jin et al., 2011). Incubating cells at 37ºC over extended periods of time may contribute to TRPV4 recycling. To examine if abolishing the temperature sensitivity of TRPV4^{FeRIC} prevents its functional downregulation, we used the temperature-insensitive mutant TRPV4$^{\Delta TFeRIC}$ (Y555A/S556A) (Duret et al., 2019; Hernández-Morales et al., 2020; Voets et al., 2002). RF stimulation significantly increased the GCaMP6 fluorescence in TRPV4$^{\Delta TFeRIC}$-expressing N2a cells imaged at either 24 or 72-h post-transfection compared with unstimulated cells (**Fig. 2A, B, table S1**; No RF 24-h: 4.3 ± 2.2; RF 24-h: 393.8 ± 62.5; No RF 72-h: 7.8 ± 3.4; RF 72-h: 399.6 ± 42.4; $p<0.0001$). RF-induced increase of GCaMP6 AUC in N2a cells expressing TRPV4$^{\Delta TFeRIC}$ was inhibited with GSK219 (**Fig. 2A, B, table S1**).

Next, we examined if lowering the extracellular Ca^{2+} levels prevents the functional downregulation of TRPV4^{FeRIC}, as it has been reported for TRPV1 (Sanz-Salvador et al., 2012b). To lower the extracellular Ca^{2+} from ~1.8 to ~0.8 mM, the TRPV4^{FeRIC}-expressing cells were incubated with culture medium supplemented with 1 mM EGTA. RF stimulation significantly increased the GCaMP6 fluorescence in EGTA-treated N2a cells expressing TRPV4^{FeRIC} imaged at either 24 or 72-h post-transfection with respect to unstimulated cells (**Fig. 2C, D, table S1**; No RF-EGTA 24-h: -5.5 ± 13; RF-EGTA 24-h: 526.2 ± 90.4; No RF-EGTA 72-h: 1.5 ± 5.4; RF-EGTA 72-h: 209.9 ± 52.8; $p<0.0001$). RF-induced increase in GCaMP6 fluorescence was larger in EGTA-treated TRPV4^{FeRIC}-expressing N2a cells relative to untreated cells (**Fig. 2C-D, insets**). Remarkably, EGTA treatment rescued the RF responsiveness in N2a cells expressing TRPV4^{FeRIC} for longer incubation periods (**Fig. 2D, table S1**).

These observations indicate that abolishing the temperature sensitivity of TRPV4^{FeRIC} or lowering the extracellular Ca^{2+} levels prevent its functional downregulation and consequent loss of RF responsiveness. Since the temperature-insensitive TRPV4$^{\Delta TFeRIC}$ is activated with RF but does not suffer downregulation, it can be an ideal candidate to be used for *in vivo* application of magnetogenetic techniques.

IV. Use of fluorescent Ca^{2+} dyes for monitoring RF-induced Ca^{2+} responses in cells expressing ferritin-tagged TRPV4

It has been reported that some Ca^{2+} dyes, such as Fura-2, may interfere with intracellular Ca^{2+} signaling (Alonso, 2003; Smith et al., 2018). Therefore, we asked if Fura-2 affects the RF-induced activation of TRPV4^{FeRIC}. N2a cells expressing GCaMP6 plus TRPV4^{FeRIC} were loaded with Fura-2 AM (1 μM) (**Fig. S4**). Because the Fura-2 excitation/emission profile is in the UV wavelength range it does not interfere with GCaMP6 emission. Fura-2 abolished the RF-induced increase in GCaMP6 AUC in TRPV4^{FeRIC}-expressing N2a cells imaged 24-h post transfection (**Fig. 2E, table S1**; RF: 550.1 ± 51; RF + Fura-2: -4.3 ± 3.9; $p<0.0001$). The inhibitory effect of

Fura-2 was corroborated in TRPV4^{FeRIC}-expressing N2a cells treated with holotransferrin and imaged 72-h post-transfection, an experimental condition that gives a robust cytosolic Ca^{2+} increase upon RF stimulation (**Fig. 2F, table S1**; RF: 226.3 ± 31.4; RF + Fura-2: 2.8 ± 6; $p<0.0001$). To examine if other Ca^{2+} indicators inhibit the RF-induced activation of TRPV4^{FeRIC}, next we monitored the cytosolic Ca^{2+} levels using the broadly used fluorescent dye Fluo-4 AM. In TRPV4^{FeRIC}-expressing N2a cells imaged 24-h post-transfection and loaded with Fluo-4, RF stimulation significantly increased the Fluo-4 fluorescence relative to unstimulated cells (**Fig. 2E, S4, table S1**; Fluo-4 No RF: 9.4 ± 2.8; Fluo-4 RF: 215.3 ± 17.9; $p<0.0001$). Remarkably, the RF-induced increase in the fluorescence of GCaMP6 and Fluo-4 were similar (**Fig. 2E, inset**). Moreover, the RF-induced increase of Fluo-4 was corroborated in N2a cells expressing TRPV4^{FeRIC} treated with holotransferrin and imaged 72-h post-transfection (**Fig. 2F, S5, table S1**). Those results indicate that, in TRPV4^{FeRIC}-expressing N2a cells, Fura-2 inhibits the RF-induced cytosolic Ca^{2+} rise whereas Fluo-4 replicates those results observed using GCaMP6 as the Ca^{2+} indicator. Those observations may guide the selection of the Ca^{2+} indicator for examining the RF-induced activation of ferritin-tagged TRPV.

V. Activation of TRPV4^{FeRIC} with RF at kHz and MHz frequencies.

It has been reported that RF waves at high kHz (Stanley et al., 2015, 2016) or MHz (Hernández-Morales et al., 2020; Hutson et al., 2017) frequencies activate ferritin-tagged TRPV. Before examining if the RF-induced activation of TRPV4^{FeRIC} depends on RF frequency, we first estimated the distribution of the electric (E) and magnetic (B) fields applied to the cells to rule out the potential contribution of the electrical field to the RF-induced Ca^{2+} responses in cells expressing TRPV4^{FeRIC}. To estimate the distribution of those fields we computed them using the finite-difference time-domain (FDTD) method implemented by the openEMS project (Liebig et al., 2013). The simulations setup included the 5 cm-diameter RF coil containing the 3.5 cm-diameter dish half-filled with imaging saline solution (dish height: 1 cm, saline solution height: 0.5 cm) (**Fig. S1C**). The dielectric constant (80) and conductivity (1.5 S/m) for the imaging saline solution was obtained from the literature (Davis et al., 2020). In the simulation, a signal with a center frequency of 180 MHz or 465 kHz was injected across the wires of a two-turn solenoid. The resulting time-domain fields were Fourier transformed, and the magnitudes of the B (T) and E (V/m) field vectors at each spatial location were calculated for 180 MHz and 465 kHz. The estimated E field corresponding to a 180 MHz and 12 μT magnetic field, at the center of the culture dish, was about 31 V/m. The estimated E field corresponding to a 465 kHz and 56 μT magnetic field, at the center of the culture dish, was about 0.29 V/m. Stimulation of RF at 465 kHz was applied at about 56 μT, because we observed that RF at lower strength did not activated the TRPV4^{FeRIC} and at larger strength (200 μT) it produces a focus drift during the imaging experiments, likely due to a heating effect on the microscope. The magnitude distribution in two dimensions, for both transverse and longitudinal cross-sections, of the magnetic and electric fields are shown in **Figure 3A - D**. As expected, the strength of the B field is relatively larger at the center of the coil/dish (**Fig. 3A, C**). In contrast, the E field amplitude drastically decreases in the center of the coil/dish (**Fig. 3B, D**). The estimated electrical field values should be negligible and should not produce significant effects on membrane ion channels. For instance, the induced potential difference between the two opposite sides of a cell membrane-embedded ion channel exposed to an E = 31 V/m is about 0.16 μV ($V_{ind}= Ed$; d is membrane thickness = 5 nm). This change (oscillating at 180 MHz) in the membrane potential is insufficient to activate voltage-gated ion channels. Importantly, the TRPV channels employed in this study are not or only

weakly voltage-dependent (Nilius et al., 2005). These estimations indicate that our RF stimulus produces negligible electrical effects on the membrane ion channels.

In TRPV4^{FeRIC}-expressing N2a cells imaged at 24-h post-transfection, RF stimulation at 180 MHz produced a robust increase of the GCaMP6 fluorescence relative to unstimulated cells (**Fig. 3E, table S1**; RF: 226.4 ± 31.4). In contrast, RF at 465 kHz and 56 μT slightly but significantly increased the GCaMP6 fluorescence relative to unstimulated cells (**Fig. 3E, table S1**; No RF 24-h: -17.4 ± 6.1; RF 24-h: 25.6 ± 8.6; $p<0.05$). To enhance the TRPV4^{FeRIC} responsiveness to RF, N2a cells were treated with holotransferrin. In those cells imaged at 72-h post-transfection, RF stimulation at 180 MHz drastically increased the GCaMP6 fluorescence (**Fig. 3F, table S1**; RF: 550.1 ± 51) relative to unstimulated cells. Although to a lesser extent, RF at 465 kHz and 56 μT also increased the GCaMP6 fluorescence relative to unstimulated cells (**Fig. 3F, table S1**; No RF + holotransferrin 72-h: -1.2 ± 4.8; RF + holotransferrin 72-h: 81.4 ± 19.4. Since the RF-induced GCaMP6 increment at 180 MHz was significantly larger (6.8 ± 0.6-fold increase; $p<0.0001$) relative to that induced at 465 KHz, our results indicate that RF is more efficient in activating TRPV4^{FeRIC} at the MHz range.

Recommendations for *in vitro* protocols to activate transiently expressed TRPV^{FeRIC} with RF waves

Based on the observations described in this report, we recommend the following protocol to use FeRIC-based magnetogenetic techniques for RF-induced activation of cells in an *in vitro* system. For a detailed methodological description, please refer to the Material and Methods section. For a detailed list of materials used in this report, please refer to Table S2.

1. In our experimental conditions, the **temperature-insensitive TRPV4$^{\Delta TFeRIC}$** produces a longer-lasting ability to remotely control cytosolic Ca^{2+} levels with RF waves than **TRPV4^{FeRIC}**.

2. Using our RF system, **RF waves at high MHz frequencies** are more efficient in increasing the cytosolic Ca^{2+} levels in cells expressing ferritin-tagged TRPV compared to RF at high kHz frequencies.

3. For monitoring RF-induced modulation of the cytosolic Ca^{2+} levels we recommend using genetically encoded Ca^{2+} indicators such as **GCAMP**.

4. For seeding, transfecting, and examining the magnetic control of ferritin-tagged TRPV we recommend the **timing protocol 1**. In this protocol, cultured cell lines are allowed to transiently express the ferritin-tagged TRPV up to 24-h post-transfection.

    i. If longer expression periods are desired, then implement recommendations 5 and 6 of this list.

5. To increase iron loading of the ferritins coupled with TRPV, supplement the culture medium with **holotransferrin (0.5 mg/mL)**. We observed that higher holotransferrin concentrations (1 and 2 mg/mL) when used with Neuro2a cells resulted in an appearance

of intracellular apoptotic-like vacuoles. It is recommended to determine the optimal concentration of holotransferrin in the particular *in vitro* system employed.

6. For those cases where it is not possible to allow short time periods of ferritin-tagged TRPV expression or supplement the culture medium with holotransferrin, the functional downregulation of those channels can be decreased by **lowering the extracellular Ca^{2+} levels**. This can be easily achieved by supplementing the culture medium with the Ca^{2+} chelator EGTA.

Discussion

Because the main components of ferritin-based magnetogenetics, including ferritin and TRPV, are subjected to a diversity of cellular regulatory mechanisms, it is crucial to unifying the experimental protocols to obtain reproducible results. The observations reported here may be used to guide the implementation of the current magnetogenetic tools.

Here we report several experimental factors that affect the RF-induced cytosolic Ca^{2+} rise in cells expressing ferritin-tagged TRPV. Those factors include the time period of $TRPV4^{FeRIC}$ expression, cellular iron import, temperature sensitivity of $TRPV4^{FeRIC}$, extracellular Ca^{2+} levels, RF frequency, and the use of different Ca^{2+} indicators. Promoting cellular iron import, mutating TRPV to abolish its temperature sensitivity or lowering extracellular Ca^{2+} levels enhance the RF-induced cytosolic Ca^{2+} rise in N2a cells expressing $TRPV4^{FeRIC}$. In contrast, longer time periods of $TRPV4^{FeRIC}$ expression and Fura-2 inhibit the RF-induced cytosolic Ca^{2+} rise in N2a cells expressing $TRPV4^{FeRIC}$. Moreover, RF waves at high MHz frequencies are more efficient in increasing the cytosolic Ca^{2+} levels in cells expressing $TRPV4^{FeRIC}$ relative to RF at high kHz frequencies.

Interestingly, longer periods of $TRPV4^{FeRIC}$ expression drastically decreases the ability of RF to produce a Ca^{2+} rise in cells expressing those channels. The possible explanations include that cellular ferritins are progressively iron-depleted, the $TRPV4^{FeRIC}$ are functionally downregulated, the coupling between ferritins and $TRPV4^{FeRIC}$ is lost, or the sum of all those factors. We have previously reported that, at the maximum period of $TRPV4^{FeRIC}$ expression tested (72-h post-transfection), the main iron-regulatory proteins mRNA are not altered by the expression of FeRIC channels (Hutson et al., 2017). This indicates that the cellular iron homeostasis is not disturbed in the FeRIC system, but it could be that those ferritins coupled to FeRIC channels are iron depleted. The potential role of the ferritin iron load in the loss of RF responsiveness was corroborated in cells treated with holotransferrin. Increasing the cellular iron import drastically enhances the RF-induced Ca^{2+} rise in cells expressing FeRIC channels at all periods tested. Remarkably, holotransferrin treatment rescued the RF responsiveness in those cells that expressed $TRPV4^{FeRIC}$ up to 72-h (**Fig. 1C**). The influence of the cellular iron import on ferritin iron load was corroborated by a recent study that reported that the ferritin iron core size depends on the presence of fetal bovine serum, ferric citrate and holotransferrin (Brier et al., 2020). Thus, the use of ferritin-based magnetogenetic tools in *in vitro* studies can be optimized by increasing the cellular iron import via holotransferrin supplementation or as reported recently, by a combination of holotransferrin and ferric citrate (Brier et al., 2020).

A crucial component of most of the magnetogenetics approaches is the TRPV channels (Chen et al., 2015; Duret et al., 2019; Hernández-Morales et al., 2020; Huang et al., 2010; Hutson et al., 2017, 2017; Stanley et al., 2015, 2016; Wheeler et al., 2016). Notably, the

functional expression of TRPV is regulated by activity-dependent mechanisms, resulting in dynamic trafficking between the cell membrane and the cytosolic vesicle pool. It has been shown that TRPV channels are maintained in vesicles and their activators cause their incorporation into the cell membrane via exocytosis (Baratchi et al., 2019; Bezzerides et al., 2004; Montell, 2004; Planells-Cases and Ferrer-Montiel, 2007). However, either constitutively or continuous activation of TRPV1 and TRPV4 causes their translocation from the cell membrane to recycling vesicles to prevent the cytotoxicity effects of excessive Ca^{2+} influx (Baratchi et al., 2019; Jin et al., 2011; Sanz-Salvador et al., 2012a; Shukla et al., 2010; Tian et al., 2019). In our FeRIC system, cells expressing $TRPV4^{FeRIC}$ are incubated at 37ºC, a temperature above the TRPV4 activation threshold (34ºC) (Huang et al., 2018; Liedtke et al., 2000; Strotmann et al., 2000). At this temperature $TRPV4^{FeRIC}$ is likely constitutively and continuously activated resulting in its functional downregulation, an effect more pronounced with longer periods of $TRPV4^{FeRIC}$ expression. The role of the temperature-mediated downregulation was corroborated with the temperature-insensitive $TRPV4^{\Delta TFeRIC}$ whose RF responsiveness was no disturbed by longer periods of expression (**Fig. 2A, B**). The functional expression of TRPV4 is also modulated by extracellular Ca^{2+} levels (Baratchi et al., 2019; Jin et al., 2011). Consistent with this finding, in our FeRIC system, lowering the extracellular Ca^{2+} levels enhances the RF responsiveness of $TRPV4^{FeRIC}$ (**Fig. 2C, D**). Therefore, our observations indicate that abolishing the temperature sensitivity of TRPV or lowering the extracellular Ca^{2+} levels prevent the functional downregulation of ferritin-tagged TRPV.

Another unexpected finding was the inhibitory effect of Fura-2 on the RF-induced cytosolic Ca^{2+} rise in N2a cells expressing $TRPV4^{FeRIC}$ (**Fig. 2E, F**). It has been reported that Fura-2 interferes with some intracellular Ca^{2+} signaling pathways (Alonso, 2003). Additionally, it has also been reported that Fluo-4 affects cell functions; nonetheless, we observed similar results using either GCaMP6 or Fluo-4 as the Ca^{2+} indicator (**Fig. 2E, F**). Therefore, it might be relevant to select a suitable Ca^{2+} indicator when examining the cytosolic Ca^{2+} rise produced by the magnetic activation of ferritin-tagged TRPV.

Although several independent studies have reported the magnetic control of TRPV1 and TRPV4 (Brier et al., 2020; Duret et al., 2019; Hernández-Morales et al., 2020; Hutson et al., 2017; Stanley et al., 2015, 2016; Wheeler et al., 2016), magnetogenetics has generated controversies about its underlying mechanisms. Some theoretical studies have suggested that the interaction between magnetic fields and ferritin could produce heat and mechanical stimuli to activate the ferritin-tagged TRPV (Barbic, 2019; Duret et al., 2019), but there is no experimental data to support those hypotheses yet. On the other hand, recent studies have postulated that a biochemical mechanism is responsible for the RF-induced activation of ferritin tagged-TRPV (Brier et al., 2020; Hernández-Morales et al., 2020). Besides this controversy, the efficacy of some ferritin-based magnetogenetics has been questioned (Kole et al., 2019; Wang et al., 2019; Wheeler et al., 2016; Xu et al., 2019). Our study indicates that several experimental factors can negatively affect the efficacy of RF waves in activating ferritin-tagged TRPV4. The observations reported here may help explain some inconsistences among different studies. However, our study is limited to the FeRIC approach with a specific transient expression of $TRPV4^{FeRIC}$, further studies are needed to corroborate our findings in other ferritin-based magnetogenetic approaches that use cells stably expressing the ferritin-tagged TRPV or chimeric ferritins.

In conclusion, our study identified several experimental factors that impact the efficacy of RF waves on inducing cytosolic Ca^{2+} rise in cells expressing ferritin-tagged TRPV. Our findings

pointed out that ferritin-based magnetogenetics are sensitive to diverse experimental factors that may disturb the functional expression and function of ferritin and/or TRPV. This study offers a guide to optimize the current ferritin-based magnetogenetic tools and protocols to obtain reproducible results.

Acknowledgements
We thank Jingjia Chen (University of California, Berkeley) for coding the customized MATLAB code for counting the number of cells for the Yo Pro 1 experiments.

Funding
Research reported in this publication was in part supported by the National Institute of Neurological Disorders and Stroke of the National Institutes of Health under Award Number R01NS110554. The content is solely the responsibility of the authors and does not necessarily represent the official views of the National Institutes of Health.

Author contributions
C.L. and M.H.-M. designed the project. M.H.-M. designed and conducted the experiments and analyses. V.H. built the RF coils and estimated the magnetic and electric field distribution in the experimental system. R.H.K. contributed to the Yo Pro experiments. M.H.-M. wrote the manuscript. C.L. and R.H.K. revised and edited the manuscript. All authors approved the manuscript.

Declaration of interests
C.L. shares ownership of a patent application (WO2016004281 A1 PCT/US2015/038948) relating to the use of FeRIC for cell modulation and treatments. All other authors declare that they have no competing interests.

Material and methods

Cell lines
Neuro2a cell line (N2a, ATC, CCL-13) was used. N2a cells were obtained from the UCB Cell Culture Facility (University of California Berkeley). Cell identity and negative Mycoplasma contamination were verified by the UCB Cell Culture Facility. Cells were maintained in Dulbeccos's Modified Eagle Medium (DMEM, Gibco) supplemented with 10% fetal bovine serum (FBS, hyclone) and 100 units/mL penicillin, and 100 mg/mL streptomycin at 37°C and 5% CO_2. For described experiments, cell lines were employed between the passages 5 to 20.

Plasmids
The constructs $TRPV4^{FeRIC}$, $TRPV4^{\Delta TFeRIC}$, and $TRPV4^{WT}$ were obtained as described previously (Hutson et al., 2017; Hernandez-Morales et al., 2020).

RF coils
For RF at the 180 MHz range, one RF emitting coil with diameter of 5 cm was used. The RF coil was made of two loops of wire. For RF at 465 kHz, one coil with a diameter of 5 cm and made of 7 loops of wire was used. The coils were connected in series with tuning capacitors forming an LC circuit, and were tuned to a resonance frequency of about 180 MHz or 465 kHz. They

were then matched to 50 ohms using parallel capacitors. For 180 MHz, the RF signal was generated by a broadband (35 MHz to 4.4 GHz) signal generator (RF Pro Touch, Red Oak Canyon LLC) and amplified using a 5W amplifier (Amplifier Research, model 5U100, 500 kHz to 1000 MHz). For 465 kHz, the RF signal was generated by a DDS signal generator and amplified using a custom-built 50W RF amplifier (operational from 100 kHz to 3 MHz). The magnetic field produced by the coils was calculated by measuring the voltage induced in a separate loop of wire connected to a high input impedance PC-based USB oscilloscope (Analog Arts model SA985) and then applying Faraday's law. For 180 MHz, care was taken to ensure that the coaxial cable from the loop of wire to the oscilloscope was half a wavelength so that the oscilloscope sees the voltage induced on the coil without interference effects. The magnetic field strength was about 12 μT or 56 μT at the position of the cell culture dishes.

Chemical transfection – Lipofectamine LTX Plus reagent

N2a cells were plated on non-coated glass-bottom 35-mm dishes. Cells were cultured in DMEM supplemented medium. After 18-24 hours, cells were transfected using the Lipofectamine LTX Plus reagent (ThermoFisher #15338030) with GCaMP6 (GCaMP6 medium, Addgene cat.40754) and TRPV4^{FeRIC} channels. For transfection, OptiMEM free serum medium (ThermoFisher #31985088) was used to prepare the DNA/Lipofectamine LTX mix. Transfection mix had the following composition per each 35-mm dish: 300 μL OptiMEM, 4 μL Lipofectamine LTX, 3 μL PLUS reagent, 0.7 μg TRPV4 DNA, and 0.7 μg of GCaMP6 DNA. Where indicated, EGTA (pH 8, ThermoFisher Scientific, #NC0997810) was added to dishes after transfection to achieve 1 mM final concentration. It was estimated that 1 mM of EGTA decreases the Ca^{2+} concentration in the DMEM culture medium from ~1.8 to ~0.8 mM (https://somapp.ucdmc.ucdavis.edu/pharmacology/bers/maxchelator/CaEGTA-TS.htm).

Protocols for seeding, transfection, and holotransferrin treatment.

Timing protocol 1 (24-h post-transfection)

N2a cells were plated on non-coated glass-bottom 35-mm dishes. Cells were cultured in DMEM supplemented medium. After 20-24 hours, cells were transfected using the Lipofectamine LTX Plus reagent (ThermoFisher #15338030) with GCaMP6 (GCaMP6 medium, Addgene cat.40754) and FeRIC channels as described above. At 20-24 h post-transfection, Ca^{2+} imaging experiments were conducted.

Timing protocol 1 (24-h post-transfection) –holotransferrin treatment

Where indicated, holotransferrin was added to culture medium immediately after transfection to achieve 0.5mg/mL final concentration. At 20-24 h post-transfection, Ca^{2+} imaging experiments were conducted.

Timing protocol 2 (48-h post-transfection)

N2a cells were seeded on 25-cm flask and cultured in DMEM supplemented medium. After 20-24 hours (day 1), cells were transfected using the Lipofectamine LTX Plus reagent (ThermoFisher #15338030) with GCaMP6 (GCaMP6 medium, Addgene cat.40754) and TRPV4^{FeRIC}. For transfection, OptiMEM free serum medium (ThermoFisher #31985088) was used to prepare the DNA/Lipofectamine LTX mix. Transfection mix had the following composition per 25-cm flask: 900 μL OptiMEM, 12 μL Lipofectamine LTX, 9 μL PLUS reagent, 2.1 μg TRPV DNA, and 2.1 μg of GCaMP6 DNA. At 24-h post-transfection, N2a cells were plated on non-coated glass-bottom 35-mm. Next, at 48-h post-transfection, Ca^{2+} imaging experiments were conducted.

Timing protocol 1 (48-h) – holotransferrin treatment

Where indicated, holotransferrin was added to culture medium immediately after transfection to achieve 0.5mg/mL final concentration. Holotransferrin treatment was maintained until Ca^{2+} imaging experiments were conducted.

Timing protocol 2 (72-h post-transfection)

N2a cells were plated on non-coated glass-bottom 35-mm dishes at very low density (1 x10E5 cells). Cells were cultured in DMEM supplemented medium. After 20-24 hours, cells were transfected using the Lipofectamine LTX Plus reagent (ThermoFisher #15338030) with GCaMP6 (GCaMP6 medium, Addgene cat.40754) and $TRPV4^{FeRIC}$ as described above. At 24-h post-transfection, the culture medium was replaced with fresh culture medium. Ca^{2+} imaging experiments were conducted at 72-h post-transfection.

Timing protocol 1 (72-h) – holotransferrin treatment

N2a cells were plated on non-coated glass-bottom 35-mm dishes at very low density (1 x10E5 cells). Cells were cultured in DMEM supplemented medium. After 20-24 hours, cells were transfected using the Lipofectamine LTX Plus reagent (ThermoFisher #15338030) with GCaMP6 (GCaMP6 medium, Addgene cat.40754) and $TRPV4^{FeRIC}$ as described above. At 24-h post-transfection, the culture medium was replaced with fresh culture medium supplemented with holotransferrin (5 mg/mL). Ca^{2+} imaging experiments were conducted at 72-h post-transfection.

Ca^{2+} imaging – GCaMP6

Epifluorescence imaging experiments were conducted as previously described (Hutson et al., 2017). Cytosolic levels of Ca^{2+} were monitored by fluorescence imaging of cells positive for GCaMP6. Cells expressing $TRPV4^{FeRIC}$ channels were identified as those cells with $mCherry^{+}$ expression. Experiments were conducted using an upright AxioExaminer Z-1 (Zeiss) equipped with a camera (Axiocam 702 mono) controlled by Zen 2.6 software. Excitation light was delivered from a LED unit (33 W/cm2; Colibri 7 Type RGB-UV, Zeiss). mCherry was excited at 590/27 nm and emission was collected at 620/60 nm. GCaMP6 was excited at 469/38 nm and emission was collected at 525/50 nm. Illumination parameters were adjusted to prevent overexposure and minimize GCaMP6 photobleaching. All the experiments corresponding to a series were done under the same illumination settings. Images were captured with a W "Plan-Apochromat" 20x/1.0 DIC D=0.17 M27 75mm lens at 1 frame/s. Experiments were carried out at room temperature (20 - 22 °C) using HBSS (Invitrogen, 14025092) that contains (in mM) 140 NaCl, 2.5 KCl, 1 $MgCl_2$, 1.8 $CaCl_2$, 20 HEPES, pH 7.3. HBSS was supplemented with 10 mM D-glucose. At the beginning of imaging experiments, a 35-mm glass-bottom dish containing the cells was washed three times with 1 mL of the HBSS. Next, the dish was placed onto the microscope stage and the cells were localized with transmitted illumination (bright field). Next, with reflected illumination, the fluorescence signals from mCherry and GCaMP6 were corroborated and the field of interest was selected. Preferred fields were those with isolated and healthy cells. A thermocouple coupled to a thermistor readout (TC-344C, Warner Instruments) was placed inside the plate in direct contact with the HBSS. The temperature of the HBSS was monitored during the experiment (Temperature initial: 22.09°C; Temperature final: 22.03°C; ΔT: -0.6°C; n=305). Cells were rested for about 10 minutes before imaging. RF was delivered using a custom-built RF-emitting coil that fits the 35-mm tissue culture dish, as described above. Cells were stimulated with RF waves at 180 MHz (at 12 μT or 56 μT) or 465 kHz (at 56 μT). For each experiment, cells were imaged for the first 60-120 s with no stimulus (Basal) and followed with RF exposure for 4-6 min. After RF stimulation, cells were exposed to GSK101, which is a TRPV

agonist, by pipetting 1 mL of the GSK101 diluted in HBSS (at 2μM) to reach the final 1μM concentration.

Ca^{2+} imaging – GCaMP6 plus Fura-2

For Fura-2 experiments, cells expressing GCaMP6 and $TRPV4^{FeRIC}$ were loaded with Fura-2. Cells were incubated with Fura-2 AM (ThermoFisher scientific, F1221) at 1 μM for 30 min at room temperature in darkness. Next, cells were washed three times with HBSS and rested for 30 min at room temperature in darkness. To corroborate cells were loaded with Fura-2, cells were imaged with a 365 nm excitation wavelength and emission was collected at 445/450 nm (**Fig. S3**). Next, cytosolic levels of Ca^{2+} were monitored by fluorescence imaging of cells positive for GCaMP6 as described in Ca^{2+} imaging – GCaMP6 section.

Ca^{2+} imaging – Fluo-4

Cytosolic levels of Ca^{2+} were monitored by fluorescence imaging of cells loaded with Fluo-4. Cells expressing $TRPV4^{FeRIC}$ were incubated with Fluo-4 AM (ThermoFisher scientific, F14201) at 10 μM for 1.5 h at room temperature in darkness. Next, cells were washed three times with HBSS and rested for 30 min at room temperature in darkness. Fluo-4 was excited at 469/38 nm and emission was collected at 525/50 nm. Illumination parameters were adjusted to prevent overexposure and minimize Fluo-4 photobleaching. All the experiments corresponding to a series were done under the same illumination settings. Images were captured with a W "Plan-Apochromat" 20x/1.0 DIC D=0.17 M27 75mm lens at 1 frame/s. Next, cytosolic levels of Ca^{2+} were monitored by fluorescence imaging of cells loaded with Fluo-4 as described in Ca^{2+} imaging – GCaMP6 section.

Yo Pro 1 assay

N2a cells were plated on non-coated glass-bottom 35-mm dishes. Cells were cultured in DMEM supplemented medium. After 18-24 hours, cells were transfected using the Lipofectamine LTX Plus reagent (ThermoFisher # 15338030) $TRPV4^{FeRIC}$ or $TRPV4^{WT}$. For transfection, OptiMEM free serum medium (ThermoFisher # 31985088) was used to prepare the DNA/Lipofectamine LTX mix. Transfection mix had the following composition per each 35-mm dish: 300 μL OptiMEM, 4 μL Lipofectamine LTX, 3 μL PLUS reagent, 0.7 μg $TRPV4^{FeRIC}$ or $TRPV4^{WT}$ DNA. After 24-hours of transfection, cells were washed three times with HBSS. Cell nuclei were stained with Hoechst 33342 (ThermoFisher Scientific, NucBlue® Live ReadyProbes® Reagent, R37605) by incubating the cells for 10 min at 37ºC. Next, cells were treated with GSK101 (50 nM or 1 μM) plus Yo Pro 1 (1 μM) for 20 min at 37ºC. Cells were washed three times with HBSS and imaged. mCherry was excited at 590/27 nm and emission was collected at 620/60 nm. Hoechst 33342 was excited at 365 nm and emission was collected at 445/50 nm. Yo Pro 1 was excited at 469/38 nm and emission was collected at 525/50 nm. For each independent experiment, cells were localized with transmitted illumination (bright field) and 2-5 fields of view were randomly selected. Cells were imaged to observe mCherry, Yo Pro 1, and Hoechst 33342 fluorescence. All the experiments were done under the same illumination settings.

Quantification and statistical analysis

Simulations of the magnetic and electric fields' produced by RF

The distribution of the electric (E) and magnetic (B) fields applied to the cells were simulated using the finite-difference time-domain (FDTD) method implemented by the openEMS project (Liebig et al., 2013) (https://openems.de/start/). The simulations were done considering the 5 cm-diameter RF coil containing the 3.5 cm-diameter dish half-filled with imaging saline solution (dish height: 1 cm, saline solution height: 0.5 cm).

Ca^{2+} imaging analysis

Cytosolic Ca^{2+} levels were monitored in cells expressing GCaMP6 and either FeRIC or wild-type TRPV channels. The fluorescence intensity of GCaMP6 was acquired at 1 Hz. GCaMP6 fluorescence was computed in a cell-based analysis with a customized MATLAB (Release 2018b, MathWorks Inc., Natick, Massachusetts) code. The maximum intensity projection was performed along the time axis to get the maximum intensity signal of cells expressing GCaMP6 in the field of view. In experiments where cells were stimulated with agonists, the maximum intensity projection corresponds to those cells which expressed functional ion channels. The watershed algorithm (MATLAB implemented function: Watershed transform)(Meyer, 1994) was used to identify and label the cells to generate a cell-based mask for each experiment. The algorithm does not contain the motion correction component because the spatial movement of cells during the time-lapse acquisition was negligible. The GCaMP6 fluorescence intensity was measured for each masked-cell of the time-lapse acquisition (600 s). GCaMP6 fluorescence signal is presented as $\Delta F/F0$, where F0 is the basal fluorescence averaged over 1-121 s before the start of stimulation and ΔF is the change in fluorescence over basal values. For analysis, the GCaMP6 fluorescence measurements corresponding to the first 5 frames were discarded because of the appearance of an inconsistent artifact. For each masked-cell, the data from 6-121 s were fit with a mono-exponential curve [f(t; a, b) = a*exp(b*t)]. The fitted curve was used to correct the GCaMP6 photobleaching effect over the entire acquisition period. The masked-cells that showed abnormal behavior, observed as the value for the growth factor (b) above 0.002, were excluded from the analysis. Masked-cells were considered responsive when the averaged $\Delta F/F0$ over time during the period from 122 to 480 s (RF-stimulation) increased 10 times over the standard deviation of the GCaMP6 $\Delta F/F0$ of the basal session. For each experimental group, the change in GCaMP6 $\Delta F/F0$ and the corresponding AUC (t = 121 – 480 s) of all analyzed masked-cells, that corresponded to all TRPV-expressing cells, were averaged. The plots of the GCaMP6 $\Delta F/F0$ changes correspond to the data obtained from all identified cells, including both responsive and non-responsive cells. The responsiveness was estimated for each independent experiment as the ratio of the responsive masked-cells relative to the total of analyzed masked-cells. For statistical analysis, the AUC (t = 122 – 480 s) was estimated for each masked-cell. Data are presented as the AUC of GCaMP6 fluorescence (± SEM), the fold change (± SEM) of the AUC of GCaMP6 fluorescence and responsiveness. The fold change was calculated by dividing the value of the AUC of GCaMP6 $\Delta F/F0$ in the presence of the stimulus (RF) by the value of that in the absence of stimulation (No stimulus or No RF). In the case fold change is less than one, the reciprocal is listed (minus-fold change). For each experimental condition, more than 3 independent experiments were conducted. The MATLAB code that we used for the Ca^{2+} imaging analysis is available in Supplementary Materials.

Yo Pro 1 assay analysis

The number of total cells (Hoechst 33342 stained cell nucleus) and the number of Yo Pro 1 positive cells in a field of view was computed in a cell-based analysis with a customized MATLAB (Release 2018b, MathWorks Inc., Natick, Massachusetts) code.

Statistical analysis

All experiments were repeated a minimum of three times. Differences in continuous data sets were analyzed using Microcal OriginPro 2020 software (OriginLab). The hypothesis testing was performed using a one-way ANOVA, followed by Tukey's post hoc test. When only two experimental groups were compared, the statistical probe applied was Student's t-test. Data are means ± SEM, where applicable $*p<0.05$, $**p<0.001$, or $***p<0.0001$ was considered a statistically significant difference.

Data and code availability

The code generated during this study is available at GitHub (https://github.com/LiuCLab/FeRIC).

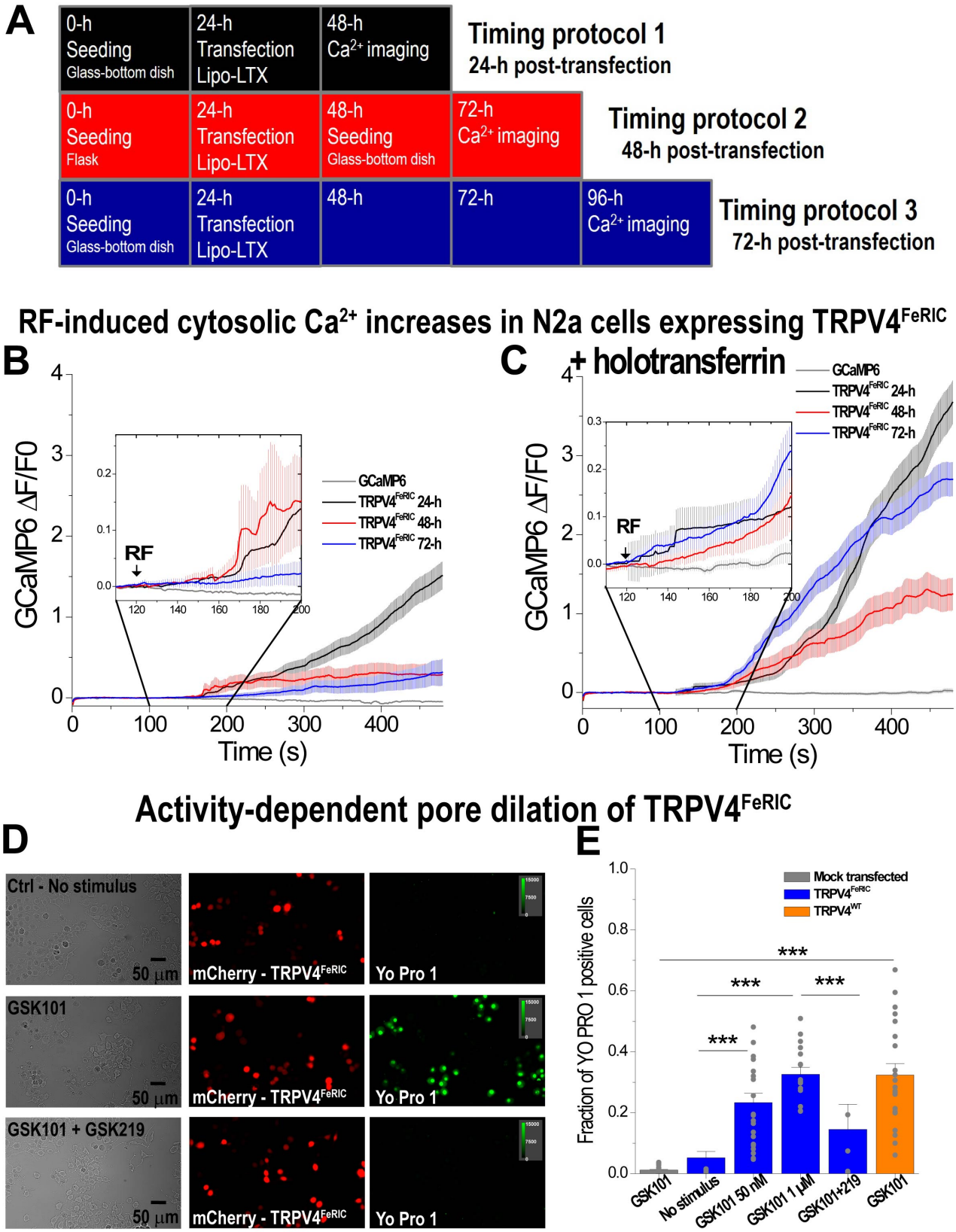
A
0-h Seeding Glass-bottom dish
24-h Transfection Lipo-LTX
48-h Ca2+ imaging
Timing protocol 1
24-h post-transfection
0-h Seeding Flask
24-h Transfection Lipo-LTX
48-h Seeding Glass-bottom dish
72-h Ca2+ imaging
Timing protocol 2
48-h post-transfection
0-h Seeding Glass-bottom dish
24-h Transfection Lipo-LTX
48-h
72-h
96-h Ca2+ imaging
Timing protocol 3
72-h post-transfection
RF-induced cytosolic Ca2+ increases in N2a cells expressing TRPV4FeRIC
B
C
+ holotransferrin
GCaMP6 ΔF/F0
Time (s)
RF
GCaMP6
TRPV4FeRIC 24-h
TRPV4FeRIC 48-h
TRPV4FeRIC 72-h
Activity-dependent pore dilation of TRPV4FeRIC
D
E
Ctrl - No stimulus
GSK101
GSK101 + GSK219
50 µm
mCherry - TRPV4FeRIC
Yo Pro 1
Mock transfected
TRPV4FeRIC
TRPV4WT
Fraction of YO PRO 1 positive cells
***
GSK101
No stimulus
GSK101 50 nM
GSK101 1 µM
GSK101+219
GSK101

1

Fig. 1. The time duration that Neuro2a cells express TRPV4^{FeRIC} influences RF-induced Ca^{2+} responses in cells expressing TRPV4^{FeRIC}. (**A**) Illustration of timing between seeding, chemical transfection and Ca^{2+} imaging of Neuro2a (N2a) cells expressing TRPV4^{FeRIC}. (**B**) Average changes (± SEM) in GCaMP6 ∆F/F0 in N2a cells expressing GCaMP6 plus TRPV4^{FeRIC} following exposure to RF at time = 120 s. Inset: zoom in of the averaged GCaMP6 ∆F/F0 before and after RF stimulation (black arrow). (**C**) Average changes (± SEM) in GCaMP6 ∆F/F0 in N2a cells expressing GCaMP6 plus TRPV4^{FeRIC} following exposure to RF (black arrow). Cells were treated with holotransferrin (0.5 mg/mL) after TRPV4^{FeRIC} transfection. Inset: zoom in of the averaged GCaMP6 ∆F/F0 before and after RF stimulation (black arrow). (**D**) Representative images of N2a cells expressing TRPV4^{FeRIC} (mCherry+) without stimulation or following GSK101 (50 nM) application for 20 min in the absence or in the presence of the TRPV4 antagonist GSK219. Scale bars = 50 µm. (**E**) Averaged fraction of N2a cells expressing TRPV4^{FeRIC} or TRPV4^{WT} that become permeable to Yo Pro 1 under different experimental conditions. The fraction of Yo Pro 1 positive cells was estimated with respect to the total number of cells in the field of view. Significance was determined using one-way ANOVA followed by Tukey's multiple comparisons test. Where applicable, either $p<0.05$ (*), $p<0.001$ (**), or $p<0.0001$ (***) was considered a statistically significant difference.

TRPV4$^{\Delta TFeRIC}$ is not functional downregulated with longer time periods of expression

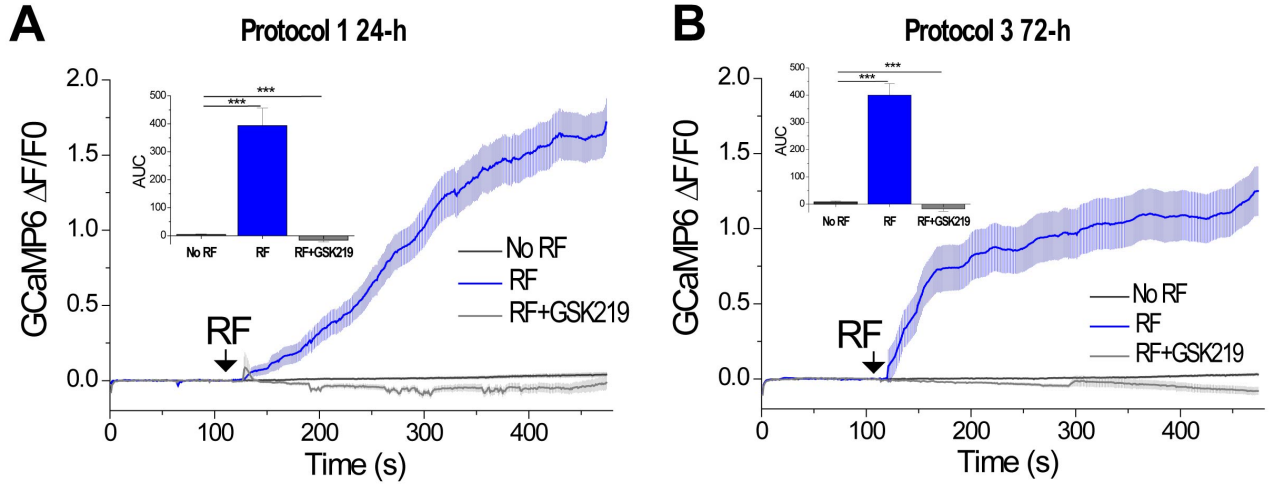

Decreasing extracellular Ca^{2+} levels prevents TRPV4^{FeRIC} functional downregulation

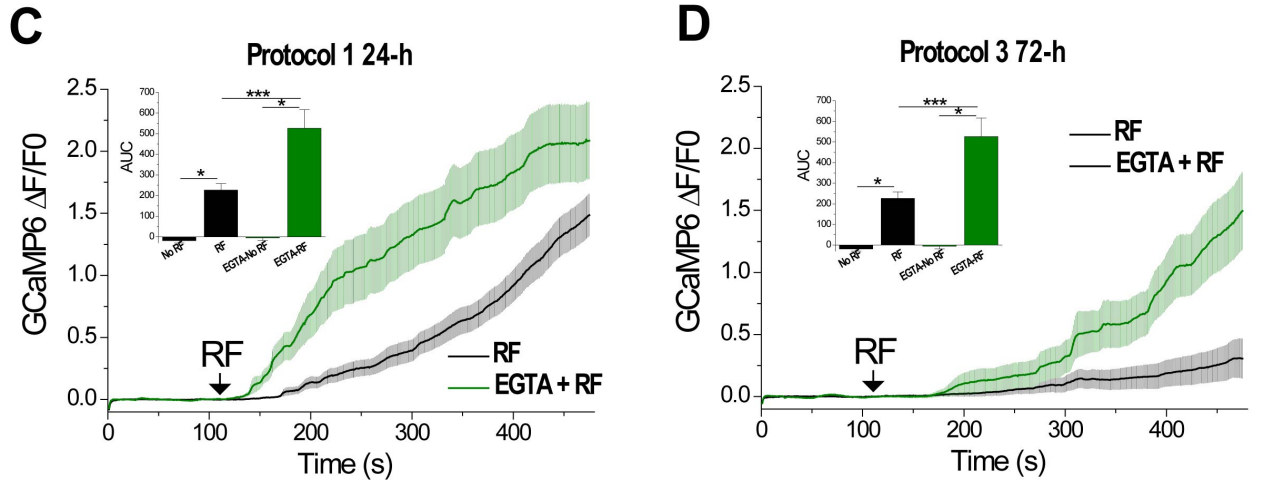

Fura-2 abolishes the RF-induced Ca^{2+} increases

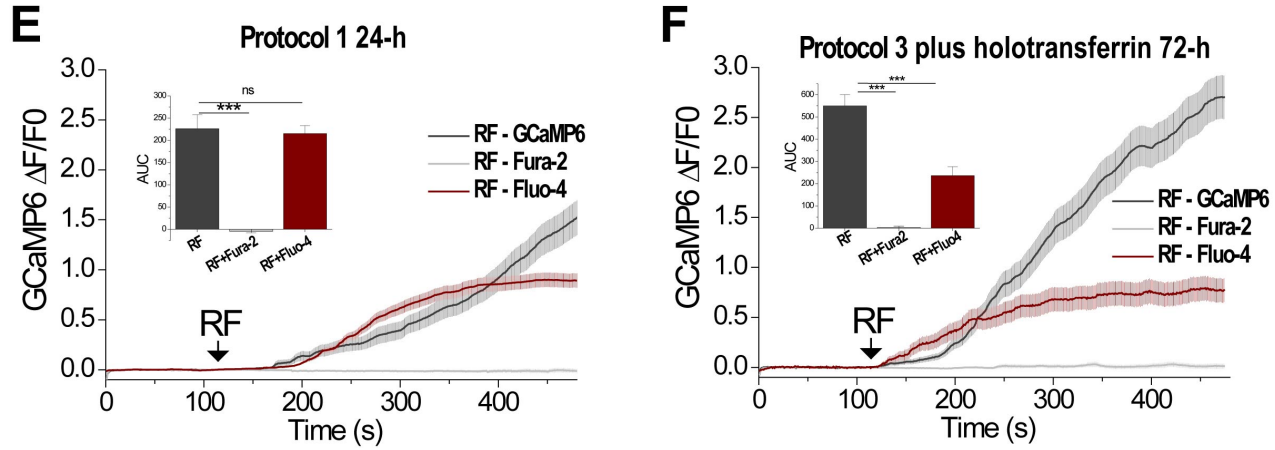

1

Fig. 2. Temperature sensitivity, extracellular Ca^{2+} levels, and Ca^{2+} indicators, impact RF-induced Ca^{2+} response in $TRPV4^{FeRIC}$. (**A, B**) Average changes (± SEM) in GCaMP6 ΔF/F0 in N2a cells expressing GCaMP6 plus $TRPV4^{\Delta TFeRIC}$ following exposure to RF (black arrows). Cells were imaged (**A**) 24-h or (**B**) 72-h post-transfection. Insets: average changes (± SEM) in GCaMP6 AUC for the period of RF stimulation. (**C, D**) Average changes (± SEM) in GCaMP6 ΔF/F0 in N2a cells expressing GCaMP6 plus $TRPV4^{FeRIC}$ following exposure to RF (180 MHz, 12 μT; black arrows). In separate experiments, cells were treated with EGTA after transfection and imaged (**C**) 24-h or (**D**) 72-h post-transfection. Insets: average changes (± SEM) in GCaMP6 AUC for the period of RF stimulation. (**E**, **F**) Average changes (± SEM) in GCaMP6 or Fluo4 ΔF/F0 in N2a cells expressing $TRPV4^{FeRIC}$ following exposure to RF (black arrows). Cells were imaged (**E**) 24-h or (**F**) 72-h post-transfection. For experiments in (**F**), culture medium was supplemented with holotransferrin. GCaMP6-expressing cells were incubated 1-h before RF stimulation with Fura2 (1μM). In separate series, cells expressing $TRPV4^{FeRIC}$ were loaded with 10 μM Fluo4 by incubation at 37ºC for 1.5-h. Insets: average changes (± SEM) in GCaMP6 or Fluo4 AUC for the period of RF stimulation. Significance was determined using one-way ANOVA followed by Tukey's multiple comparisons test. Where applicable, either $p<0.05$ (*), $p<0.001$ (**), or $p<0.0001$ (***) was considered a statistically significant difference.

A Magnetic field (T), **RF 180 Mhz**

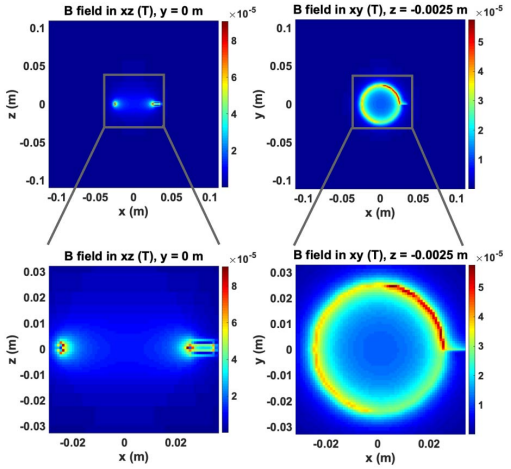

B Electric field (V/m), **RF 180 MHz**

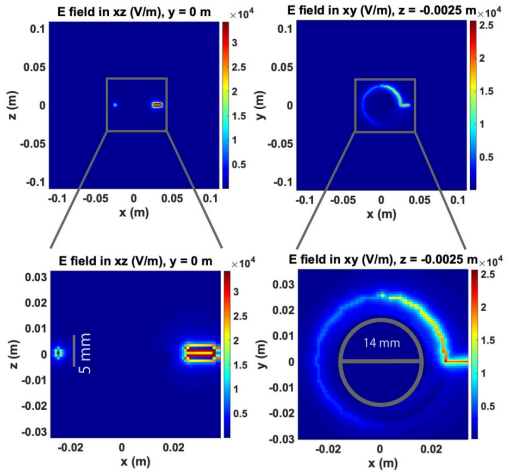

C Magnetic field (T), **RF 465 kHz**

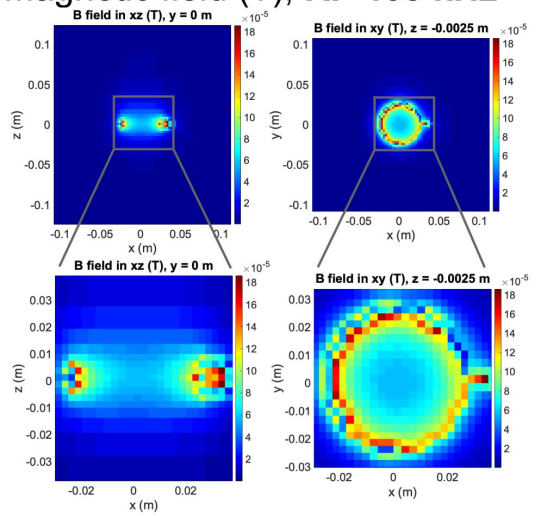

D Electric field (V/m), **RF 465 kHz**

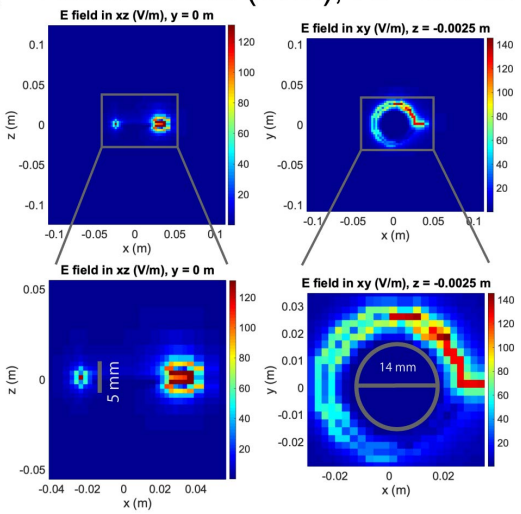

Cytosolic Ca^{2+} increases generated by RF at MHz and KHz frequencies

E

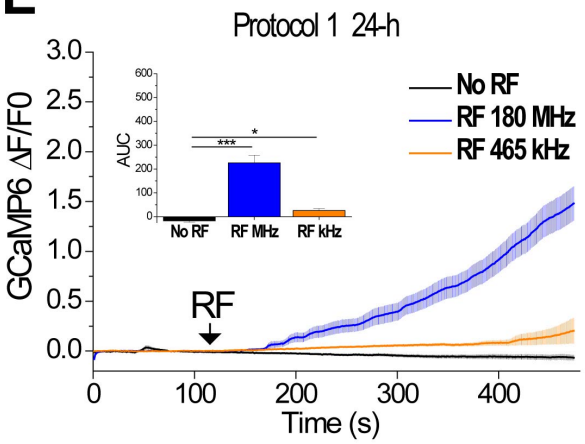

F

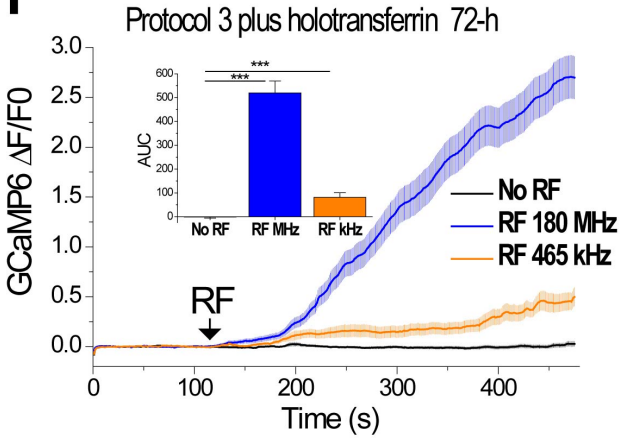

1

Fig. 3. RF stimulation at MHz frequency produces larger cytosolic Ca^{2+} increases with respect to RF at kHz frequency. (**A**, **C**) Simulations of the magnetic and electric fields' produced by RF**.** Distribution of the magnetic field in the culture dish produced by RF waves at (**A**) 180 MHz and 12 μT or (**C**) 465 kHz and 56 μT; bottom: zoom in of the culture dish. (**B**, **D**) Distribution of the E field in the culture dish (hall-filled with saline solution) produced by RF waves at (**B**) 180 MHz and 12 μT or (**D**) 465 kHz and 56 μT; bottom: zoom in of the culture dish. Vertical lines correspond to the 5mm-height of the saline solution being in the lower half of the coil. The grey circle corresponds to the glass area where the cells are cultured. (**E, F**) Average changes (± SEM) in GCaMP6 $\Delta F/F0$ in N2a cells expressing GCaMP6 plus $TRPV4^{FeRIC}$ following exposure to RF at 180 MHz and 12 μT or RF at 465 kHz and 56 μT (black arrows). Cells were imaged (**E**) 24-h or (**F**) 72-h post-transfection. Insets: average changes (± SEM) in GCaMP6 AUC for the period of RF stimulation. For experiments in (**F**), culture medium was supplemented with holotransferrin. Insets: average changes (± SEM) in GCaMP6 AUC for the period of RF stimulation. Significance was determined using one-way ANOVA followed by Tukey's multiple comparisons test. Where applicable, either $p<0.05$ (*), $p<0.001$ (**), or $p<0.0001$ (***) was considered a statistically significant difference.

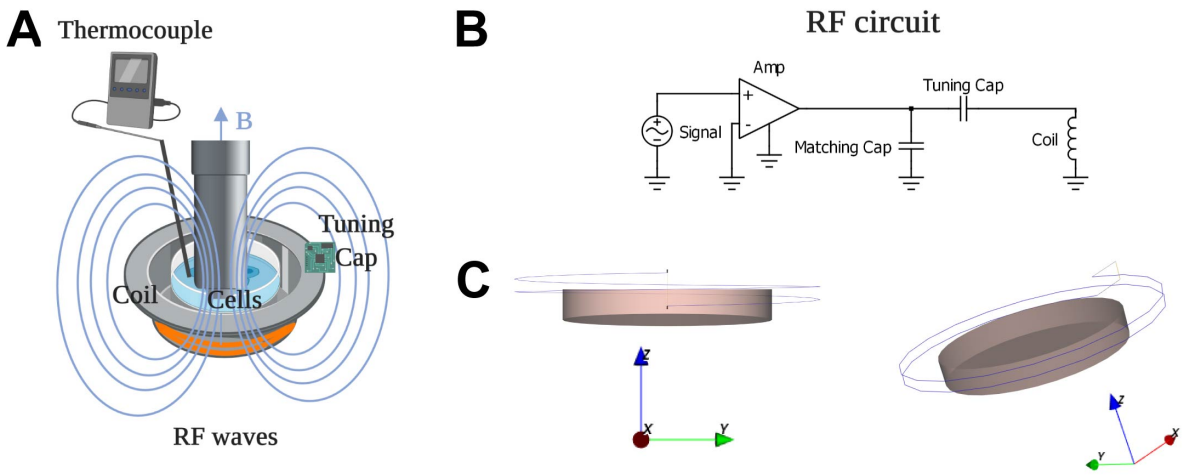

Fig. S1. Scheme of the RF setup. (**A**) Illustration of the experimental set up for RF stimulation of cultured cells. (**B**) RF circuit. (**C**) Two orientations of 3D models of the culture dish and the solenoid RF coil.

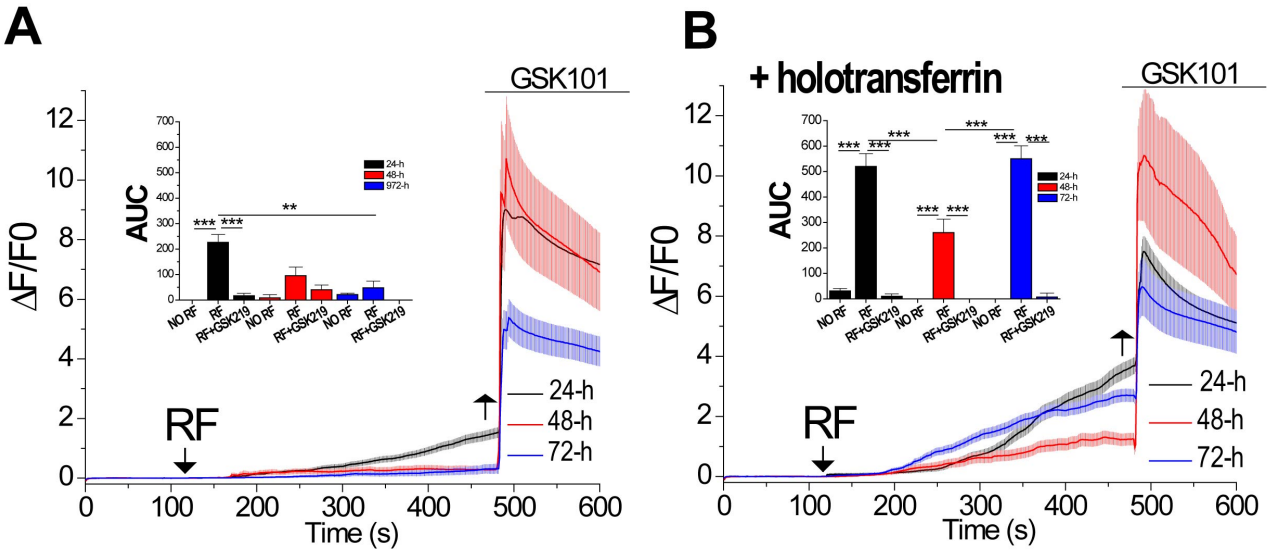

Fig. S2. RF-induced Ca^{2+} responses in N2a cells expressing $TRPV4^{FeRIC}$. (**A**) Average changes (± SEM) in GCaMP6 ΔF/F0 in N2a cells expressing GCaMP6 plus $TRPV4^{FeRIC}$ following exposure to RF (black arrows) and then GSK101 (solid line). Inset: average changes (± SEM) in GCaMP6 AUC for the period of RF stimulation. (**B**) Average changes (± SEM) in GCaMP6 ΔF/F0 in N2a cells expressing GCaMP6 plus $TRPV4^{FeRIC}$ following exposure to RF (black arrows) and then GSK101 (solid line). Cells were treated with holotransferrin (0.5 mg/mL) after $TRPV4^{FeRIC}$ transfection. Inset: average changes (± SEM) in GCaMP6 AUC for the period of RF stimulation. Significance was determined using one-way ANOVA followed by Tukey's multiple comparisons test. Where applicable, either $p<0.05$ (*), $p<0.001$ (**), or $p<0.0001$ (***) was considered a statistically significant difference.

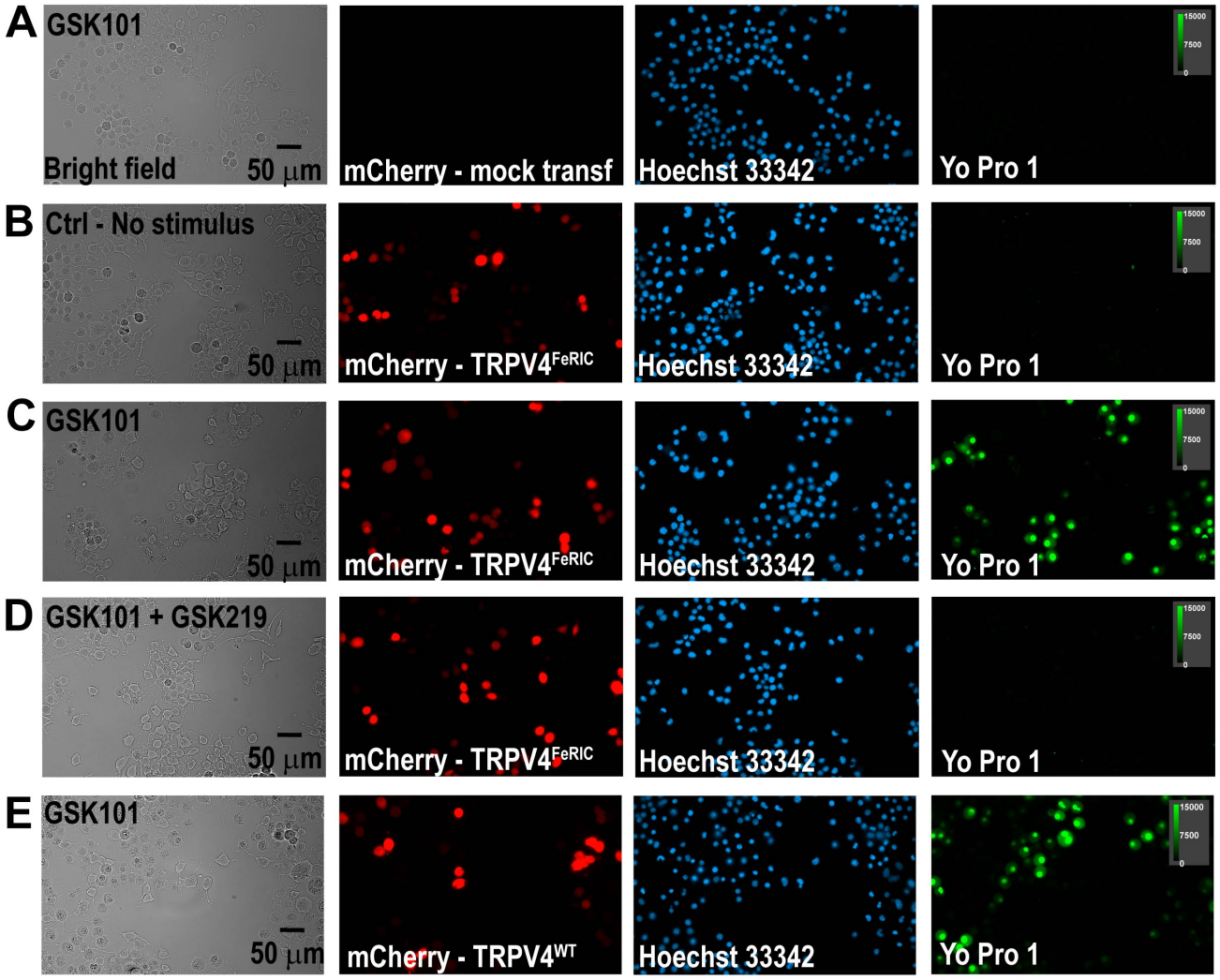

Fig. S3. Continuous stimulation with GSK101 dilates the TRPV4^{FeRIC} pore allowing Yo Pro 1 influx. (**A - E**) Representative images of N2a cells mock-transfected or expressing TRPV4^{FeRIC} or TRPV4^{WT} (mCherry+). Cell nuclei were labeled with Hoechst 33342 (blue emission). After GSK101 treatment, cells were to detect Yo Pro 1 (green emission) fluorescence. Control experiments correspond to (**A**) mock-transfected N2a cells stimulated with GSK101 or (**B**) non-stimulated TRPV4^{FeRIC}-expressing cells. N2a cells expressing (**C**) TRPV4^{FeRIC} or (**E**) TRPV4^{WT} were treated with GSK101 100 nM for 20 min at 37ºC. In a separate series of experiments, (**D**) N2a cells expressing TRPV4^{FeRIC} were treated with the specific TRPV4 antagonist GSK219 (1 μM) 10 min before agonist stimulation. Scale bars = 50 μm.

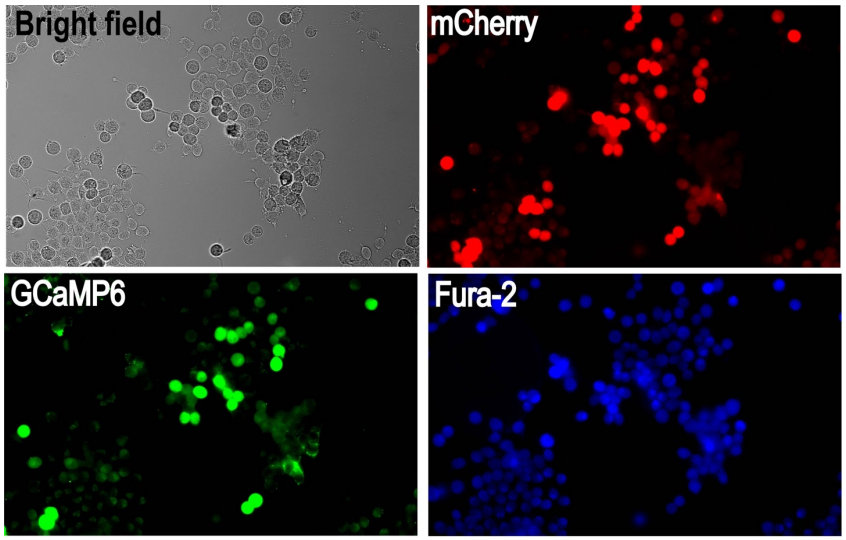

Fig. S4. Representative images of N2a cells expressing TRPV4^{FeRIC} (mCherry^{+}) plus GCaMP6 and loaded with Fura-2 (1 μM).

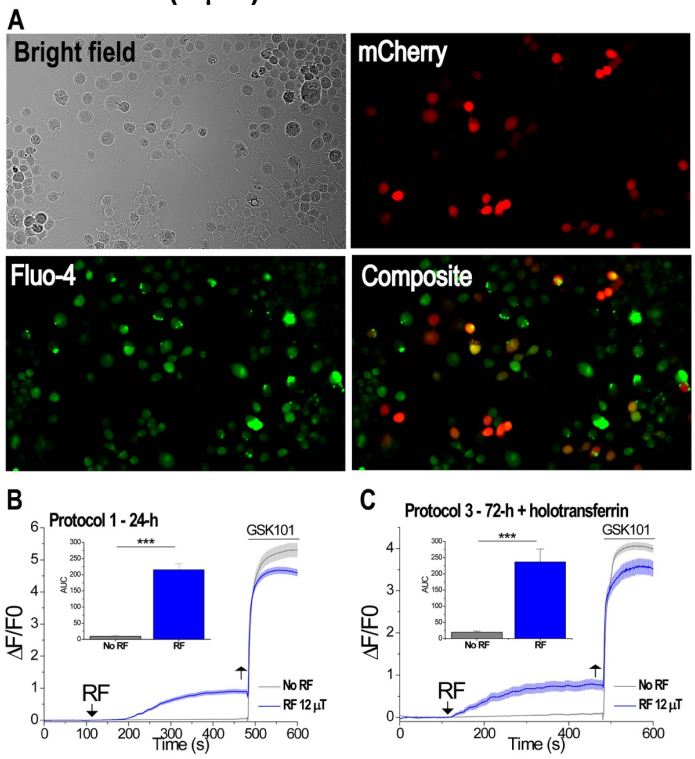

Fig. S5. RF increases the Fluo4 fluorescence in N2a cells expressing TRPV4^{FeRIC}. (A) Representative images of N2a cells expressing TRPV4^{FeRIC} (mCherry^{+}) and loaded with Fluo4 (1 μM). (**B, C**) Average changes (± SEM) in Fluo4 ΔF/F0 in N2a cells expressing TRPV4^{FeRIC} following exposure to RF at 180 MHz and 12 μT (black arrows) and next GSK101 (solid line). Cells were imaged (**B**) 24-h or (**C**) 72-h (plus holotransferrin) post-transfection. Insets: average changes (± SEM) in Fluo4 AUC corresponding to the period of RF stimulation.

Experimental group	AUC (± SEM)	Fraction of responsive cells (± SEM)	N= number independent experiments	n= number of cells
Neuro2a cells expressing GCaMP6 plus TRPV4^{FeRIC} – Timing protocol 1 – 24 h post-transfection				
TRPV4^{FeRIC} - No RF	-17.4 ± 6.1	0.19 ± 0.11	4	161
TRPV4^{FeRIC}- RF 12 µT (180 MHz)	226.4 ± 31.4	0.43 ± 0.12	5	289
TRPV4^{FeRIC}- RF 12 µT (180 MHz) + GSK219	16.8 ± 9.9	0.19 ± 0.04	4	94
Neuro2a cells expressing GCaMP6 plus TRPV4^{FeRIC} – Timing protocol 1 – 24 h post-transfection plus holotransferrin				
TRPV4^{FeRIC} - No RF	31 ± 9.5	0.27 ± 0.06	5	113
TRPV4^{FeRIC}- RF 12 µT (180 MHz)	520 ± 50.2	0.52 ± 0.14	7	164
TRPV4^{FeRIC}- RF 12 µT (180 MHz) + GSK219	10.2 ± 9.5	0.35 ± 0.18	5	38
Neuro2a cells expressing GCaMP6 plus TRPV4^{FeRIC} – Timing protocol 2 – 48 h post-transfection				
TRPV4^{FeRIC} - No RF	8.5 ± 12.9	0.23 ± 0.08	5	45
TRPV4^{FeRIC}- RF 12 µT (180 MHz)	95.5 ± 34	0.27 ± 0.10	6	67
TRPV4^{FeRIC}- RF 12 µT + (180 MHz) GSK219	40.4 ± 19	0.35 ± 0.17	6	55
Neuro2a cells expressing GCaMP6 plus TRPV4^{FeRIC} – Timing protocol 2 – 48 h post-transfection plus holotransferrin				
TRPV4^{FeRIC} - No RF	-0.5 ± 7.3	0.14 ± 0.05	5	81
TRPV4^{FeRIC}- RF 12 µT	260.6 ± 52.9	0.43 ± 0.16	5	113
TRPV4^{FeRIC}- RF 12 µT + GSK219	-12.6 ± 6.8	0.07 ± 0.04	5	83
Neuro2a cells expressing GCaMP6 plus TRPV4^{FeRIC} – Timing protocol 3 – 72 h post-transfection				
TRPV4^{FeRIC} - No RF	21.1 ± 5.8	0.12 ± 0.08	5	111
TRPV4^{FeRIC}- RF 12 µT (180 MHz)	48.1 ± 26.2	0.3 ± 0.07	9	114
TRPV4^{FeRIC}- RF 12 µT (180 MHz) + GSK219	-11.2 ± 6.3	0.02 ± 0.02	8	80
Neuro2a cells expressing GCaMP6 plus TRPV4^{FeRIC} – Timing protocol 3 – 72 h post-transfection plus holotransferrin				
TRPV4^{FeRIC} - No RF	-1.2 ± 4.8	0.1 ± 0.03	11	329
TRPV4^{FeRIC}- RF 12 µT (180 MHz)	550.1 ± 51	0.66 ± 0.09	9	219
TRPV4^{FeRIC}- RF 12 µT (180 MHz) + GSK219	7.2 ± 15.8	0.1 ± 0.05	8	80

Neuro2a cells expressing GCaMP6 plus TRPV4$^{\Delta TFeRIC}$ – Timing protocol 1 – 24 h post-transfection				
TRPV4$^{\Delta TFeRIC}$ - No RF	4.3 ± 2.2	0.23 ± 0.04	5	318
TRPV4$^{\Delta TFeRIC}$ - RF 12 µT (180 MHz)	393.8 ± 62.5	0.52 ± 0.06	4	236
TRPV4$^{\Delta TFeRIC}$ - RF 12 µT + (180 MHz) GSK219	-15.8 ± 6.9	0.1 ± 0.03	4	167
Neuro2a cells expressing GCaMP6 plus TRPV4$^{\Delta TFeRIC}$ – Timing protocol 3 – 72 h post-transfection				
TRPV4$^{\Delta TFeRIC}$ - No RF	7.8 ± 3.4	0.27 ± 0.08	4	70
TRPV4$^{\Delta TFeRIC}$ - RF 12 µT (180 MHz)	399.6 ± 42.4	0.57 ± 0.13	6	247
TRPV4$^{\Delta TFeRIC}$ - RF 12 µT (180 MHz) + GSK219	-17.2 ± 8.8	0.37 ± 0.23	4	53
Neuro2a cells expressing GCaMP6 plus TRPV4^{FeRIC} – Timing protocol 1 – 24 h post-transfection – EGTA treatment				
TRPV4^{FeRIC} - No RF + EGTA	-5.5 ± 13	0.28 ± 0.14	3	29
TRPV4^{FeRIC}- RF 12 µT (180 MHz) + EGTA	526.2 ± 90.4	0.53 ± 0.16	4	93
Neuro2a cells expressing GCaMP6 plus TRPV4^{FeRIC} – Timing protocol 3 – 72 h post-transfection – EGTA treatment				
TRPV4^{FeRIC} - No RF + EGTA	1.46 ± 5.4	0.1 ± 0.07	5	89
TRPV4^{FeRIC}- RF 12 µT (180 MHz) + EGTA	209.9 ± 52.8	0.32 ± 0.08	7	102
Neuro2a cells expressing GCaMP6 plus TRPV4^{FeRIC} – Timing protocol 1 – 24 h post-transfection + Fura-2				
TRPV4^{FeRIC} - RF 12 µT (180 MHz)	-4.3 ± 3.9	0.17 ± 0.04	4	202
Neuro2a cells expressing TRPV4^{FeRIC} loaded with Fluo-4 – Timing protocol 1 – 24 h post-transfection				
TRPV4^{FeRIC} - RF 12 µT (180 MHz)	215.3 ± 17.8	0.44 ± 0.14	4	602
Neuro2a cells expressing GCaMP6 plus TRPV4^{FeRIC} – Timing protocol 3 – 72 h post-transfection + holotransferrin + Fura-2				
TRPV4^{FeRIC} - RF 12 µT	2.8 ± 6	0.1 ± 0.1	4	120
Neuro2a cells expressing TRPV4^{FeRIC} loaded with Fluo-4 – Timing protocol 3 – 72 h post-transfection + holotransferrin				
TRPV4^{FeRIC} - RF 12 µT	236.4 ± 40.1	0.5 ± 0.1	3	274

Neuro2a cells expressing GCaMP6 plus TRPV4^{FeRIC} – Timing protocol 1 – 24 h post-transfection – RF at 465 kHz frequency				
TRPV4^{FeRIC} - RF 56 µT (465 kHz)	25.6 ± 8.6	0.31 ± 0.2	5	93
Neuro2a cells expressing GCaMP6 plus – Timing protocol 3 – 72 h post-transfection – + holotransferrin RF at 465 kHz frequency				
TRPV4^{FeRIC} - RF 56 µT (465 kHz)	81.4 ± 19.4	0.32 ± 0.11	5	106

Table S1. GCaMP6 data from N2a cells expressing TRPV4^{FeRIC}. GCaMP6 data were quantified as the change in GCaMP6 fluorescence divided by baseline fluorescence (ΔF/F0). For each experimental condition, listed here is the averaged GCaMP6 area under the curve (AUC) ± SEM, the fraction of cells responsive to RF or lipids, the number of separate experiments (N), and number of analyzed cells (n).

REAGENT or RESOURCE	SOURCE	IDENTIFIER
Chemicals		
Opti-MEM™ I Reduced Serum Medium, no phenol red	Thermo Fisher Scientific	14025092
HBSS, calcium, magnesium, no phenol red	Thermo Fisher Scientific	A14291DJ
Lipofectamine™ LTX Reagent with PLUS™ Reagent	Thermo Fisher Scientific	A12621
Penicillin-Streptomycin (10,000 U/mL)	Thermo Fisher Scientific	15140122
Fetal Bovine Serum, qualified, heat inactivated, United States	Thermo Fisher Scientific	16140071
DMEM, high glucose, GlutaMAX™ Supplement	Thermo Fisher Scientific	10566016
Trypsin-EDTA (0.25%), phenol red	Thermo Fisher Scientific	25200056
GSK1016790A	Sigma-Aldrich	G0798
GSK 2193874	TOCRIS	5106
holo-Transferrin human	Sigma-Aldrich	T0665
EGTA Buffer 0.5M, pH 8.0	Thermo Fisher Scientific	NC0997810
Experimental Models: Cell Lines		
Neuro-2a	ATCC	CCL-131
Recombinant DNA		
Rat TRPV4 (TRPV4^{WT}) pLVX-Ef1a-TRPV4^{WT}-IRES-mCherry	Hutson et al., 2017	n/a
Rat TRPV4^{FeRIC} pLVX-Ef1a-TRPV4^{FeRIC}-IRES-mCherry	Hutson et al., 2017	n/a

Rat TRPV4$^{\Delta TFeRIC}$ Y555A/S556A pLVX-Ef1a-TRPV4$^{\Delta TFeRIC}$-IRES-mCherry	Hernández-Morales et al., 2020	n/a
GCaMP6m	Addgene	#40754
Software		
ZEN 2.6	Zeiss	https://www.zeiss.com/microscopy/us/downloads.html
ImageJ	NIH	https://imagej.nih.gov/ij/index.html
SERIAL CLONER 2.6	SerialBasics	http://serialbasics.free.fr/Home/Home.html
MATLAB R2018b	MathWorks, USA	https://www.mathworks.com/products/matlab.html
Origin 7	OriginLab, MA	https://www.originlab.com/
BioRender	BioRender	https://biorender.com/
Adobe Illustrator®	Adobe	https://www.adobe.com/creativecloud.html

Table S2. List of the chemicals, cell lines, recombinant cDNA, and software used in this report.

References

Alonso, M. (2003). Fura-2 antagonises calcium-induced calcium release. Cell Calcium *33*, 27–35.

Banke, T.G., Chaplan, S.R., and Wickenden, A.D. (2010). Dynamic changes in the TRPA1 selectivity filter lead to progressive but reversible pore dilation. American Journal of Physiology-Cell Physiology *298*, C1457–C1468.

Baratchi, S., Keov, P., Darby, W.G., Lai, A., Khoshmanesh, K., Thurgood, P., Vahidi, P., Ejendal, K., and McIntyre, P. (2019). The TRPV4 Agonist GSK1016790A Regulates the Membrane Expression of TRPV4 Channels. Front. Pharmacol. *10*, 6.

Barbic, M. (2019). Possible magneto-mechanical and magneto-thermal mechanisms of ion channel activation in magnetogenetics. ELife *8*, e45807.

Bezzerides, V.J., Ramsey, I.S., Kotecha, S., Greka, A., and Clapham, D.E. (2004). Rapid vesicular translocation and insertion of TRP channels. Nat Cell Biol *6*, 709–720.

Brier, M.I., Mundell, J.W., Yu, X., Su, L., Holmann, A., Squeri, J., Zhang, B., Stanley, S.A., Friedman, J.M., and Dordick, J.S. (2020). Uncovering a possible role of reactive oxygen species in magnetogenetics. Sci Rep *10*, 13096.

Chen, R., Romero, G., Christiansen, M.G., Mohr, A., and Anikeeva, P. (2015). Wireless magnetothermal deep brain stimulation. Science *347*, 1477–1480.

Davis, H.C., Kang, S., Lee, J.-H., Shin, T.-H., Putterman, H., Cheon, J., and Shapiro, M.G. (2020). Nanoscale Heat Transfer from Magnetic Nanoparticles and Ferritin in an Alternating Magnetic Field. Biophysical Journal *118*, 1502–1510.

Dunn, K.M., Hill-Eubanks, D.C., Liedtke, W.B., and Nelson, M.T. (2013). TRPV4 channels stimulate Ca2+-induced Ca2+ release in astrocytic endfeet and amplify neurovascular coupling responses. Proceedings of the National Academy of Sciences *110*, 6157–6162.

Duret, G., Polali, S., Anderson, E.D., Bell, A.M., Tzouanas, C.N., Avants, B.W., and Robinson, J.T. (2019). Magnetic Entropy as a Proposed Gating Mechanism for Magnetogenetic Ion Channels. Biophysical Journal *116*, 454–468.

Ferrandiz-Huertas, C., Mathivanan, S., Wolf, C., Devesa, I., and Ferrer-Montiel, A. (2014). Trafficking of ThermoTRP Channels. Membranes *4*, 525–564.

Ferreira, L.G.B., and Faria, R.X. (2016). TRPing on the pore phenomenon: what do we know about transient receptor potential ion channel-related pore dilation up to now? J Bioenerg Biomembr *48*, 1–12.

Giometto, B., Gallo, P., and Tavolato, B. (1993). Transferrin Receptors in the Central Nervous System. In Methods in Neurosciences, (Elsevier), pp. 122–134.

Grosse, C., and Schwan, H.P. (1992). Cellular membrane potentials induced by alternating fields. Biophysical Journal *63*, 1632–1642.

Hernández-Morales, M., Shang, T., Chen, J., Han, V., and Liu, C. (2020). Lipid Oxidation Induced by RF Waves and Mediated by Ferritin Iron Causes Activation of Ferritin-Tagged Ion Channels. Cell Reports *30*, 3250-3260.e7.

Huang, H., Delikanli, S., Zeng, H., Ferkey, D.M., and Pralle, A. (2010). Remote control of ion channels and neurons through magnetic-field heating of nanoparticles. Nature Nanotech *5*, 602–606.

Huang, R., Wang, F., Yang, Y., Ma, W., Lin, Z., Cheng, N., Long, Y., Deng, S., and Li, Z. (2018). Recurrent activations of transient receptor potential vanilloid-1 and -4 promote cellular proliferation and migration in esophageal squamous cell carcinoma cells. FEBS Open Bio 2211-5463.12570.

Hutson, M.R., Keyte, A.L., Hernández-Morales, M., Gibbs, E., Kupchinsky, Z.A., Argyridis, I., Erwin, K.N., Pegram, K., Kneifel, M., Rosenberg, P.B., et al. (2017). Temperature-activated ion channels in neural crest cells confer maternal fever–associated birth defects. Sci. Signal. *10*, eaal4055.

Jin, M., Wu, Z., Chen, L., Jaimes, J., Collins, D., Walters, E.T., and O'Neil, R.G. (2011). Determinants of TRPV4 Activity following Selective Activation by Small Molecule Agonist GSK1016790A. PLoS ONE *6*, e16713.

Kole, K., Zhang, Y., Jansen, E.J.R., Brouns, T., Bijlsma, A., Calcini, N., Yan, X., Lantyer, A. da S., and Celikel, T. (2019). Assessing the utility of Magneto to control neuronal excitability in the somatosensory cortex. Nat Neurosci.

Kotnik, T., Bobanović, F., and Miklavcˇicˇ, D. (1997). Sensitivity of transmembrane voltage induced by applied electric fields—A theoretical analysis. Bioelectrochemistry and Bioenergetics *43*, 285–291.

Liebig, T., Rennings, A., Held, S., and Erni, D. (2013). openEMS - a free and open source equivalent-circuit (EC) FDTD simulation platform supporting cylindrical coordinates suitable for the analysis of traveling wave MRI applications: openEMS-A FREE AND OPEN SOURCE EC FDTD SIMULATION PLATFORM. Int. J. Numer. Model. *26*, 680–696.

Liedtke, W., Choe, Y., Martí-Renom, M.A., Bell, A.M., Denis, C.S., Sali, A., Hudspeth, A.J., Friedman, J.M., and Heller, S. (2000). Vanilloid receptor-related osmotically activated channel (VR-OAC), a candidate vertebrate osmoreceptor. Cell *103*, 525–535.

McCoy, D.D., Palkar, R., Yang, Y., Ongun, S., and McKemy, D.D. (2017). Cellular permeation of large molecules mediated by TRPM8 channels. Neuroscience Letters *639*, 59–67.

Meyer, F. (1994). Topographic distance and watershed lines. Signal Processing *38*, 113–125.

Montell, C. (2004). Exciting trips for TRPs. Nat Cell Biol *6*, 690–692.
Nilius, B., Talavera, K., Owsianik, G., Prenen, J., Droogmans, G., and Voets, T. (2005). Gating of TRP channels: a voltage connection?: Voltage dependence of TRP channels. The Journal of Physiology *567*, 35–44.
Planells-Cases, R., and Ferrer-Montiel, A. (2007). TRP Channel Trafficking. In TRP Ion Channel Function in Sensory Transduction and Cellular Signaling Cascades, W.B. Liedtke, and S. Heller, eds. (Boca Raton (FL): CRC Press/Taylor & Francis), p.
Sanz-Salvador, L., Andrés-Borderia, A., Ferrer-Montiel, A., and Planells-Cases, R. (2012a). Agonist- and Ca^{2+} -dependent Desensitization of TRPV1 Channel Targets the Receptor to Lysosomes for Degradation. J. Biol. Chem. *287*, 19462–19471.
Sanz-Salvador, L., Andrés-Borderia, A., Ferrer-Montiel, A., and Planells-Cases, R. (2012b). Agonist- and Ca^{2+} -dependent Desensitization of TRPV1 Channel Targets the Receptor to Lysosomes for Degradation. J. Biol. Chem. *287*, 19462–19471.
Shen, J., Tu, L., Chen, D., Tan, T., Wang, Y., and Wang, S. (2019). TRPV4 channels stimulate Ca2+-induced Ca2+ release in mouse neurons and trigger endoplasmic reticulum stress after intracerebral hemorrhage. Brain Research Bulletin *146*, 143–152.
Shukla, A.K., Kim, J., Ahn, S., Xiao, K., Shenoy, S.K., Liedtke, W., and Lefkowitz, R.J. (2010). Arresting a Transient Receptor Potential (TRP) Channel: β-ARRESTIN 1 MEDIATES UBIQUITINATION AND FUNCTIONAL DOWN-REGULATION OF TRPV4. J. Biol. Chem. *285*, 30115–30125.
Stanley, S.A., Sauer, J., Kane, R.S., Dordick, J.S., and Friedman, J.M. (2015). Remote regulation of glucose homeostasis in mice using genetically encoded nanoparticles. Nat Med *21*, 92–98.
Stanley, S.A., Kelly, L., Latcha, K.N., Schmidt, S.F., Yu, X., Nectow, A.R., Sauer, J., Dyke, J.P., Dordick, J.S., and Friedman, J.M. (2016). Bidirectional electromagnetic control of the hypothalamus regulates feeding and metabolism. Nature *531*, 647–650.
Strotmann, R., Harteneck, C., Nunnenmacher, K., Schultz, G., and Plant, T.D. (2000). OTRPC4, a nonselective cation channel that confers sensitivity to extracellular osmolarity. Nature Cell Biology *2*, 695–702.
Taghian, T., Narmoneva, D.A., and Kogan, A.B. (2015). Modulation of cell function by electric field: a high-resolution analysis. J. R. Soc. Interface *12*, 20150153.
Tian, Q., Hu, J., Xie, C., Mei, K., Pham, C., Mo, X., Hepp, R., Soares, S., Nothias, F., Wang, Y., et al. (2019). Recovery from tachyphylaxis of TRPV1 coincides with recycling to the surface membrane. Proc Natl Acad Sci USA *116*, 5170–5175.
Voets, T., Prenen, J., Vriens, J., Watanabe, H., Janssens, A., Wissenbach, U., Bödding, M., Droogmans, G., and Nilius, B. (2002). Molecular Determinants of Permeation through the Cation Channel TRPV4. J. Biol. Chem. *277*, 33704–33710.
Wang, G., Zhang, P., Mendu, S.K., Wang, Y., Zhang, Y., Kang, X., Desai, B.N., and Zhu, J.J. (2019). Revaluation of magnetic properties of Magneto. Nat Neurosci.
Wheeler, M.A., Smith, C.J., Ottolini, M., Barker, B.S., Purohit, A.M., Grippo, R.M., Gaykema, R.P., Spano, A.J., Beenhakker, M.P., Kucenas, S., et al. (2016). Genetically targeted magnetic control of the nervous system. Nat Neurosci *19*, 756–761.
Xu, F.-X., Zhou, L., Wang, X.-T., Jia, F., Ma, K.-Y., Wang, N., Lin, L., Xu, F.-Q., and Shen, Y. (2019). Magneto is ineffective in controlling electrical properties of cerebellar Purkinje cells. Nat Neurosci.